




University of
Stavanger

Faculty of Science and Technology

MASTER'S THESIS

Study program/Specialization: MSc in Engineering Structures and Materials Specialization: Mechanical systems	Spring semester, 2020 Open access
Writer: Simen Rasmussen	 (Writer's signature)
Faculty supervisor: Hirpa G. Lemu External supervisors: Ole Gabrielsen (DNV GL), Andreas Aaslid (DNV GL)	
Thesis title: Finite Element Modelling and Analysis of Axial Settlement of Light Poles	
Credits (ECTS): 30	
Key words: <ul style="list-style-type: none">- Slip joint- Axial settlement- Light poles- Abaqus- Non-linear finite element analysis	Pages: 62 + enclosure: 14 Stavanger, 28.06.20 Date/year

**FINITE ELEMENT MODELLING
AND ANALYSIS
OF AXIAL SETTLEMENT
OF LIGHT POLES**

Preface

This master's thesis has been written in cooperation with DNV GL during the spring semester of 2020 at the Department of Mechanical and Structural Engineering and Materials Science at the University of Stavanger.

I would like to thank Ole Gabrielsen and Andreas Aaslid at DNV GL, and Hirpa G. Lemu at University of Stavanger for guidance throughout the thesis. Writing the thesis in cooperation with DNV GL has been experiencing, although the spring of 2020 has been a different and challenging period due to the covid-19 outbreak.

Abstract

The slip joint technology is a method for connecting two conical pole segments together, without the use of bolts or grout, thus reducing time of installation and the need of maintenance. In recent years there have been an urge to apply this technology offshore, however there is generally little knowledge about its behavior. Furthermore, slip joint connections have been found to experience axial settlement over time. In this thesis detailed numerical analysis of the settlement phenomena of tall masts using slip joint connections has been performed.

The phenomenon has been studied by creating a light pole model, in finite element software Abaqus, which has been simulated with the full loading procedure consisting of pre-loading, upending and a series of storms, representing wind loads from several years of operation. Parameter studies has been performed where the influence of pre-load force and coefficient of friction on axial settlement have been analyzed.

Results showed that axial settlement occurred in the slip joint connection throughout the whole simulation procedure. With increased pre-load force, the slip joint connection experienced less axial settlement afterwards. Smaller coefficient of friction resulted in larger axial settlement both during pre-loading and afterwards. Therefore, it has been concluded that both pre-load force and the coefficient of friction affects the axial settlement in a slip joint connection.

Table of Contents

Preface.....	i
Abstract	ii
Table of Contents	iii
1 Introduction	1
1.1 Background.....	1
1.2 Problem definition	2
1.3 Aim	2
1.4 Objectives	3
1.5 Limitations.....	3
2 A literature study on slip joints	4
2.1 Introduction	4
2.2 Design of slip joints.....	4
2.2.1 General design considerations.....	4
2.2.2 Design loads	5
2.2.3 Geometry	5
2.2.4 Contact	6
2.2.5 Friction	6
2.2.6 Design approaches.....	6
2.3 Assembling of slip joints	7
2.4 Description of slip joints in standards	8
2.4.1 Relevant standards.....	8
2.4.2 Offshore standards.....	10
2.4.3 American standards	10
2.5 Summary.....	10
3 Methodology	12
3.1 General.....	12
3.2 Preparatory work	12
3.3 Finite element modelling and analysis	12
3.3.1 Parameter study	13
4 Identification of key parameters.....	14
4.1 Overall dimensions	14
4.2 Dissimilar tapers	14
4.3 Material properties.....	15
4.4 Coefficient of friction	15

4.5	Orientation of light poles relative to dominant wind direction.....	16
4.6	Effect of temperature	18
4.7	Jacking tension during assembling.....	18
4.8	Misalignment of cross-sections during assembling.....	18
5	Manual calculations.....	19
5.1	Purpose of the manual calculations	19
5.2	Case 1: Friction between a body and inclined plane	19
5.3	Case 2: Compound cylinder	20
5.3.1	Theory	20
5.3.2	Calculating axial movement as a result of assembling	21
5.3.3	Calculating for a more significant axial displacement.....	22
5.4	Case 3: Thin-walled cylindrical shell under axisymmetric loading	22
6	Finite Element Modelling and Analysis.....	24
6.1	Introduction	24
6.2	A brief description of the masts.....	24
6.3	Loading procedure.....	26
6.3.1	Pre-loading	26
6.3.2	Upending	26
6.3.3	Wind loads.....	26
6.4	Material definition	30
6.4.1	Elasticity and plasticity	30
6.4.2	Density	31
6.5	Simple model.....	32
6.5.1	General	32
6.5.2	Geometry.....	32
6.5.3	Mesh and element type.....	33
6.5.4	Boundary conditions	33
6.5.5	Contact formulation.....	33
6.5.6	Comparing results to manual calculations	34
6.6	Setup of the realistic model	38
6.6.1	General	38
6.6.2	Model geometry	38
6.6.3	Element types	39
6.6.4	Mesh.....	40
6.6.5	Contacts.....	40

6.6.6	Steps	42
6.6.7	Loads and boundary conditions.....	42
6.7	About the parameter studies	45
6.7.1	Study 1: Variations of pre-loading	45
6.7.2	Study 2: Variations of coefficients of friction.....	45
7	Results from Finite Element Analyses	46
7.1	Maximum stresses during assembling and upending	46
7.1.1	Results of pre-loading	46
7.1.2	Stresses during upending.....	47
7.2	Result of static wind loads.....	48
7.3	Axial settlement with quasi-static wind loads	49
7.4	Parameter study 1: Pre-load force	50
7.5	Parameter study 2: Coefficient of friction	51
8	Conclusions and Further Work	53
8.1	Conclusions	53
8.2	Further work	53
	References	54
	Appendix 1: Pole taper calculation.....	56
	Appendix 2: Manual calculation of friction.....	57
	Appendix 3: Manual calculation of compound cylinder.....	59
	Appendix 4: Thin-walled cylindrical shell.....	65
	Appendix 5: Wind load calculation.....	69

1 Introduction

1.1 Background

During an inspection of the light poles on a stadium, deformations were observed on some of the ladders attached to the light poles. These, originally straight, ladders had been bent and some of the brackets attaching them to the pole structure had either been deformed or completely torn off. One of the deformed ladders, which had experienced inward bending, can be seen in Fig. 1. In Fig. 2, one of the torn off ladder brackets is shown.

The inspected light poles each consist of five shorter pole segments, assembled to form a 47 m tall structure. The bottom four segments are connected in series with use of slip joints: a technology used for connecting two conical mast segments together without use of bolts, grout or similar. An example that can portray the concept of a slip joint connection is two paper cups, upside down, being placed on top of one another. This concept is shown in Fig. 3. Due to the conical shape of the cups, the upper cup is prevented from moving downwards once in place. If one were to forcefully push the cups tightly together, one would experience that pulling the cups apart afterwards becomes more difficult. This is due to the frictional forces acting on the surfaces in which the cups are in contact.

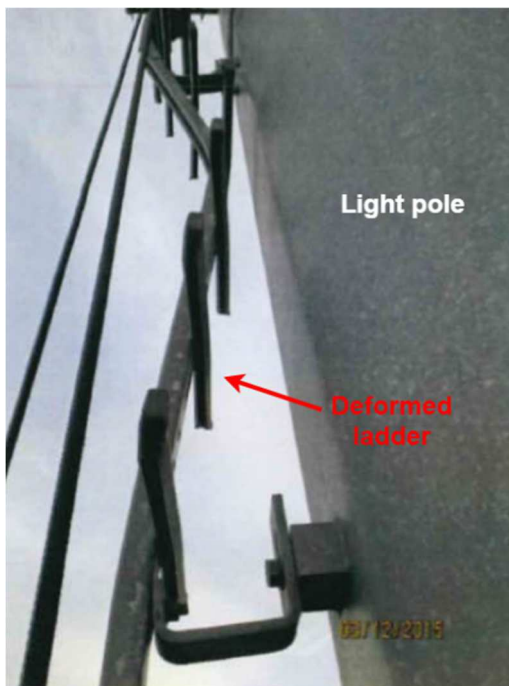


Fig. 1 – Picture of a deformed ladder attached to one of the light poles, taken during the inspection (DNV GL, 2015).

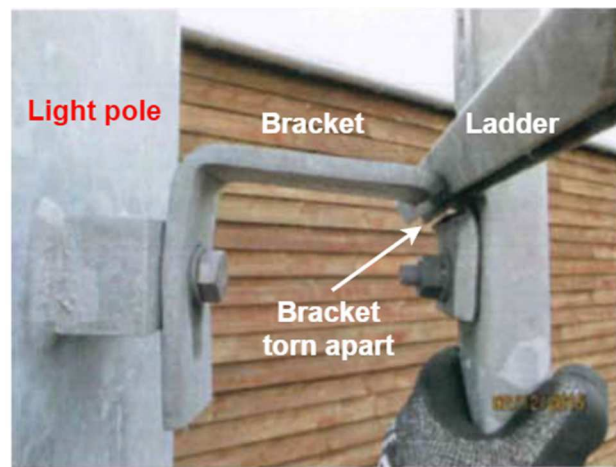


Fig. 2 – Picture of one of the brackets attaching a ladder to the light pole, taken during the inspection (DNV GL, 2015). The image shows that the bracket section bolted to the ladder has been completely torn apart from the rest of the bracket.

In essence, the paper cup analogy can be used to describe the slip joint. The bottom segment of the slip joint is fitted inside the upper segment, both of which are conical with practically equal cone angles. During assembling of a slip joint, the two segments are forced together so that the friction forces acting on shared surfaces, prevent the parts from separating at a later stage. Upon contact of the two segments, the sections must deform slightly in the radial direction to

accommodate the mismatch of diameters between the parts. Essentially an interference fit is formed, meaning that the nominal outer diameter of the bottom segment is slightly larger than the nominal inner diameter of the top segment. Thus, the inner section is in compression, while the outer section is in tension. As the parts are pulled further towards each other, the mismatch of the interference fit increases, yielding increased interfacial pressure.

An evaluation of the condition of the light poles performed in 2015 by DNV GL, concluded that the light poles were intact and that axial settlement at the slip joint connections was the most likely explanation for the ladder deformations. Further settlement was expected to either be slowed down or halted due to the conical shape of the segments (DNV GL, 2015).

The slip joints are commonly used for light poles and tall masts in civil engineering. Lately, the slip joint technology has been used for offshore wind projects as well and has potential to save installation time compared to conventional bolted joints. In general, there is little knowledge about the behavior of the slip joint connection and detailed numerical analysis of the settlement phenomena for the current light poles has not been performed to date.

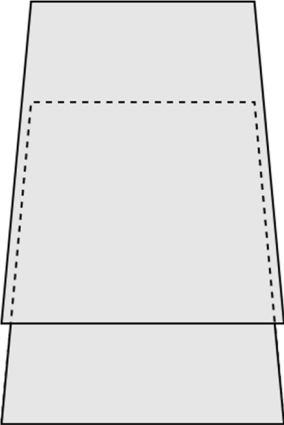


Fig. 3 - The principle of a slip joint connection: one conical mast segment is fitted inside another conical mast segment.

1.2 Problem definition

The central problem of this thesis is to perform detailed numerical analysis of the settlement phenomena of tall masts using slip joint connections. Since deformations were observed at the slip joints, these are areas of interest that require special attention. There is a need to investigate what could trigger the axial settlement of the poles, both in terms of the design and their method of assembly.

1.3 Aim

The aim of the thesis is to study the observed settlement phenomena of the light poles by using finite element simulations.

1.4 Objectives

- Gain knowledge on different aspects of design and assembly of slip joints, including their description in standards.
- Identify key parameters for light poles and slip joints that could influence the extent of axial settlement.
- Build a finite element (FE) model of the light pole using a non-linear finite element software. The FE software shall as a minimum provide support for material non-linearity and contact.
- Establish a load sequence simulating the whole load history from assembly, upending and several years of operation.
- Perform parameter studies to see which parameter could trigger axial settlement at the slip joints.

1.5 Limitations

There are some limitations in this thesis related to the modelling and simulation of the floodlight mast. Firstly, not so much effort has been put into modelling mast regions far from the studied slip joint. This is due to the slip joint being the region of interest in this thesis. The fact that only one slip joint is included in the model may yield different results than if all three slip joints were modelled. However, the neglected slip joints were the ones that had experienced less axial settlement and therefore it has been assumed that these were tightly assembled prior to operation. Also, dealing with three slip joint connections opposed to one would likely result in unnecessary long simulation times.

Throughout the modelling, geometric variations within fabrication tolerances have not been considered, meaning that the mast has been modelled based on nominal values. For instance, variations of the pole diameters could greatly influence the behaviour of the slip joint connections with regards to axial settlement. Also, the pole cross-sections are in reality not perfect 16-sided polygons as in the models, which could influence the contact obtained in a slip joint connection.

The applied wind loads have merely been modelled to represent a few large storms and not the whole wind history from several years of operation. Thus, any axial settlement caused by the many high-frequency oscillations of the structure has not been involved in the analyses. However, the large storms have been applied to investigate stresses in the slip joint region and whether the light pole model experience axial settlement. A more realistic wind load history could aid any future investigation of slip joint connections.

2 A literature study on slip joints

2.1 Introduction

The central problem of this thesis is to study the settlement phenomena experienced on light poles where slip joint technology is used. In 2015, DNV GL performed an assessment of light poles with said characteristics, where axial settlement had been observed. The report concluded that the settlement had occurred in the slip joint connections (DNV GL, 2015). A prerequisite for performing finite element simulations and analysis of light poles where slip joints are present, is insight on the various aspects of the connection type. This literature study on slip joints will cover some design aspects and assembly procedures, along with a review of its recognition in standards.

The slip joint has been in use for several decades in utility poles, light poles and wind turbine support structures, and in recent years an urge has arose to apply this technology for offshore wind turbines. The 30th of September 2018, the first offshore wind turbine using slip joint technology was installed off the coast of Ijmuiden in Netherlands, set to collect data and be used for testing (Sif Group, 2018). This was an important step in the process of obtaining more knowledge about the slip joint, especially about its behavior in rougher environments. Although the slip joint principle has been known for many years, there have generally been little effort devoted to the testing and research of it (Slocum and Fairbairn, 2015).

One of the reasons as to why the slip joint connection is an attractive technology is partly due to its simple geometry, which could save time in terms of fabrication, installation and maintenance, generally meaning lowered costs. The conical shape of the segments is what nullifies the need for bolts, grout or welds in ensuring a tightly fitted connection. A manufacturer of wind turbines in Netherlands, named WindMaster, spent one fourth of the time assembling a slip joint mast compared to one assembled with conventional methods (van der Tempel and Lutje Schipholt, 2003). Sif Group who are working with foundations for offshore wind turbines, explains that the high maintenance level in general is caused by the bolts fixing transition pieces to monopiles. A mentioned alternative is grouted connections, but they were found to settle over time. However, the introduction of slip joints would not require bolts or grout, thus removing some of the related problems (Sif Group, n.d.).

2.2 Design of slip joints

2.2.1 General design considerations

There are several aspects to consider when a slip joint connection is to be designed. Firstly, they must function with their intended purpose, which is to tightly connect two pole segments. An improper connection may potentially possess an increased risk of failure, which can be both dangerous and costly. The safety is of special importance when the structure is placed in the vicinity of human activity, such as for light poles. The slip joint must be designed so that it is able to withstand environmental loads from the surroundings. In this there also lies that the lifetime is not reduced due to shortcomings of the design. Although the slip joint is a relatively straightforward concept, the geometric parameters must be considered with care.

2.2.2 *Design loads*

The slip joint will be subject to its self-weight and exposed to environmental loads, although the extent of the latter depends on its application and local conditions. All the loads affecting the structure and the behavior of the slip joint must be taken into consideration in the design process. In cases of tall masts, the overturning moment can become substantial and therefore the slip joint must be able to transfer these loads. Wind loads will generally be the main contributing part to the overturning moment and can also cause vibrations in the structure. The ever-present self-weight can at times be accompanied by loads caused by snow or ice, that further magnifies the downward acting force. For design of slip joints that are intended for offshore structures, the effect of waves must also be considered. Maximum expected loads have generally been the foundation for pole structure design, where the calculations of stresses are based on elastic analysis (Dicleli and Nassar, 2003).

2.2.3 *Geometry*

The two separate slip joint members are essentially just a section of the pole, and thus the pole design influences the characteristics of the slip joint. The cross-sectional shape of structural poles can vary from rectangular to polygonal and circular, but in general, the steel tubular poles have polygonal cross-sections with number of sides ranging from 6 to 24 depending on pole thickness and diameter (Dicleli and Nassar, 2003). The maximum thickness of the pole can be limited by the machine bending flat plates into tubular structures. Although thicker walls yield a stronger pole, it also means a heavier structure consisting of more material which consequently puts additional weight on the slip joints. If the pole structure is to be galvanized in a pool, this may also set limitations for maximum diameter and length of the pole segment.

An important feature of poles with slip joints is the cone angle, as it will slow down axial sliding of the upper pole section. Upon contact, the pole segment must accommodate its complementary part by slightly deforming, to slide further. A study of the slip joint with finite element analyses, performed by Segeren et al. (2014), found that long overlaps combined with small cone angles were ideal for carrying loads from the upper to the bottom piece. The cone angle was described to ideally be less than 2° and the overlap length 1.5 times the diameter (Segeren et al., 2014). A drawback of small cone angles is that theoretically less radial deformation is necessary for axial settlement to occur.

Two pole segments with equal taper will in theory fit perfectly together and be in full contact throughout the contact surfaces. However, in reality there are a lot of uncertainties and the pole angles are likely to deviate slightly from their nominal values. Segeren (2018) investigated this issue, and when the angle of the upper segment was larger than the bottom segment, a gap at the lower end of the slip joint was expected. In the opposite case, when the angle of the upper segment was smaller than the bottom segment, a gap is initially apparent at the top of the slip joint. This gap can however be expected to diminish as the segments are forced together and the upper pole section is deformed (Segeren, 2018). To ensure full contact between the segments, it may be beneficial to design the upper pole segment with slightly smaller cone angle than the bottom part.

The overlapping length of the slip joint determines the amount of nominal contact surface that can transfer the loads between the segments. The upper segment has a diameter slightly larger

than the bottom so that the bottom segment fits inside the upper. Larger differences in these diameters results in longer overlaps. The design overlap length is often defined in terms of the diameter, so that poles of large diameters require longer overlaps. American standards recommend slip joint lengths of 1.5 times the diameter, likely based on experience (Slocum and Fairbairn, 2015). This number was the same in the previously discussed project, of Segeren (2014), but with the explanation that this is the ratio used for grouted connections (Segeren et al., 2014). Although defining the overlap in terms of the diameter may result in conservative design in some cases, there are uncertainties related to the coefficient of friction and the actual amount of contact between the segments, both of which influence the carrying capabilities of the connection.

2.2.4 Contact

Inside the slip joint the pole segments are in contact, and the contact surface is ideally consistent throughout the overlap length. This may however not be the case with different load scenarios and geometric variations within the tolerances. Segeren (2018) performed an experiment on a slip joint where the contact between the cones was investigated. The conical sections were measured and based on these measurements, initial points for contact during assembly were predicted. With a highly accurate measuring laser, the distance between the laser and the inside of the slip joint was found. This process produced rings of data points and was repeatedly performed stepwise throughout the length of both slip joint parts. The data sets were placed together to see where contact initiated. As the data sets were moved closer together, resembling the two slip joint parts pulled together, contact spread from its initial point. (Segeren, 2018) The experiment can highlight the importance of obtaining the desired overlapping length to ensure that the slip joint is in proper contact throughout. As the two slip joint parts are pulled tighter together, they are likely to undergo deformation and subsequently the contact area will increase. In the design of a slip joint there is important to consider the tolerances of the geometry, to avoid large discrepancies in the geometry from the manufacturing side. However, fabrication tolerances for the poles is not something that will be investigated further in this thesis.

2.2.5 Friction

Between the two slip joint surfaces in contact, friction forces resisting relative motion of the segments will arise. Friction is dependent on several factors, and the coefficient of friction can change remarkably with only small deviations from the test conditions (Oberg, 2012). In many cases where the slip joint technology is applied, the structure is galvanized with a protective layer of zinc. Static friction for clean zinc-on-zinc connections is stated to be 0.6 (Oberg, 2012, p. 166). In the design of a slip joint the uncertainty of the coefficient of friction must be taken into consideration. The friction force is determined by the normal force acting on the slip joint surfaces in contact. This normal force will depend on the cone angle and will be amplified by the surface pressure generated as the segments are forced together.

2.2.6 Design approaches

Dicleli and Nassar (2003) developed a computer-aided approach for designing tubular steel poles with slip joints. Reduction of weight is desired in an optimum design, and therefore their design approach involved making the pole structure as lightweight as possible, while tolerating

certain load cases. Through a trial and error approach, over 100 various poles differing in diameter and taper was investigated to find the optimum design. Results from the algorithm were plotted in charts, where the diameter was plotted as a function of the moment at the base. (Dicleli and Nassar, 2003) Such plots can be useful for optimizing the pole structure in terms of diameter, but the study did not investigate the slip joint in particular, as the poles only consisted of one segment.

A project which studied the slip joint, was performed by the Dutch Offshore Wind Energy Converter (DOWEC), where the design document of a WindMaster wind turbine was investigated. Design of the slip joint connection was based on two loads, namely gravity and overturning moment. Friction forces were neglected in the calculations due to the assumption that when friction is considered, calculated stresses in the structure will decrease. Therefore, neglecting the effect of friction was a conservative assumption affecting the internal stress calculation. (van der Tempel and Lutje Schipholt, 2003) Although the final formula for calculating stresses in the section contains thickness, slip joint length and cone angle, it is not dependent of diameter of the slip joint.

2.3 Assembling of slip joints

The slip joint is assembled by letting the two separate tubular structures slide together. To ensure proper connection, application of axial forces is required in order to overcome the friction forces between the two members. The minimum overlapping length presumably decided in the design phase, must be reached. A proper fit may also minimize further unwanted slip. There are various methods of forcing the two slip joints sections together, some of which are described in this section.

DOWEC investigated an onshore wind turbine utilizing slip joints that had been assembled by dropping the upper segment onto the lower. First the lower pole section had been bolted to the foundation and followingly the upper pole segment had been dropped onto the lower, forming a slip joint connection with an overlapping length of 3 m. In the dropping procedure, the upper pole section had been raised just a few centimeters from where it was in contact with the bottom part and then instantaneously released. Upon impact it had virtually gained a downward linear momentum, thus slipping further than without an initial velocity. The final step in the assembling was to mount the nacelle and the wind turbine blades, effectively adding more weight to the slip joint. After eight years of operation, in 2003 when DOWEC investigated the wind turbine, the slip joint had settled axially by less than 5 cm (van der Tempel and Lutje Schipholt, 2003). When the site was revisited in 2011, no further settlement could be observed (Segeren, 2018). This creates a reason to believe that axial settlement following the assembly procedure, eventually will halt due to the conical shape of the connection.

The method of dropping the upper pole section onto the other may in some cases be inappropriate, for instance for offshore installations due to the unpredictable nature of wind and waves. It is crucial that the structure is not damaged during installation, as it can shorten its lifetime or functionality. As knowledge about the behavior of slip joint is somewhat limited, achieving a tight fit throughout the length of the connection is necessary, especially in the harsh offshore environment. A more controlled manner of installation is preferable in many cases, both to avoid local damage of the structure and to ensure proper contact between the segments.

Another investigation of slip joints, performed by Segeren et al. (2014), compared the achieved slip length with and without initial velocities as well as proposing an alternative. By numerical calculation the method of assembly having zero initial velocity and relying entirely on self-weight, was found to only yield tiny slip lengths. In the second case the initial velocity was set to 1.4 m/s, intended to resemble the velocity of the pole after accelerating from a 10 cm drop. Expectedly, the axial displacement was found to be greater in the latter case. However, neither of the cases resulted in slip lengths that could be deemed satisfactory. Therefore, another method of assembly was proposed, where harmonic loads were applied in the axial direction of the pole. Numerous simulations of 90 seconds of loading were performed, where the harmonic load was differing in amplitude and frequency. The desired axial settlement was reached for several frequency-amplitude pairings and could possibly become a viable installation method. In the offshore industry a comparable technique is already in use, namely, installation of piles by vibratory drivers (Segeren et al., 2014). Selection of assembly method may also be dictated by availability of equipment. It is advantageous if vibratory drivers already available for pile driving also can be used to assemble slip joint connections.

In the DOWEC project previously described, another method for assembling slip joints was mentioned. Rather than dropping the upper pole section and letting it accelerate, assembling with use of hydraulic jacks was suggested. These hydraulic jacks could pull the upper pole section further upon the lower segment. This method of assembly is described to have resulted in quite significant additional slippage of more than 20 cm when the wind turbine nacelle and blades are placed on top (van der Tempel and Lutje Schipholt, 2003). However, the extent of axial settlement following the assembly may be due to lacked pre-stressing of the connection.

Trinity Meyer is a supplier of such hydraulic jacking units, that has described the procedure of assembling the slip joint. While laying horizontally, one segment is slid onto the other before the jacking equipment is attached. Prior to the jacking process, the centerlines of the pole sections must be aligned. It is also important that all hydraulic jacks are pulling with the same force, to prevent the pole to lean towards one side. During upending their equipment is able to hold the segments together, meaning that they cannot slip apart and resettle later. Although the jacking procedure described is performed horizontally, this can be done vertically as well (Trinity Meyer, n.d.). If the slip joint is to be joined with jacking devices, points of attachment must be added near the splices during manufacturing. These attachments can be nuts, in which bolts are inserted during the jacking procedure (Barone, 2014).

2.4 Description of slip joints in standards

2.4.1 Relevant standards

Standards that may be of relevance for slip joints are briefly investigated in this section. The original design for the light poles situated at the stadium, were projected based on three standards, namely DIN 4131, DIN 18800 and DIN 1055-4 (DNV GL, 2015). These are German standards which respectively describes steel radio towers and masts, steel structures and lastly, wind loads on structures. DNV GL however, based their verification on a newer standard, NS-EN 1991-1-4, which encompasses actions on structures (DNV GL, 2015) and is incorporated in the Eurocode 1. The NS-EN 1991-1-4 standard describes wind actions specifically, and

includes calculation for polygon shaped structural elements as well as circular cylinders (Standard Norge, 2005a).

Eurocode 3 is a standard for design of steel structures, and part 1-8 of this standard encompasses design of joints (Standard Norge, 2005b). Although many connection methods are described, no mention of slip joint is made. Part 3-1 of the Eurocode 3 is devoted to towers, masts and chimneys (Standard Norge, 2005c). This part of the standard similarly fails to mention the slip joint.

Another relevant standard is the NS-EN 40 which describes lighting columns. Throughout this standard, no mention of slip joint is made. However, the standard merely describes lighting columns up to 20 m tall (Standard Norge, 1992). Connection dimensions for lanterns is described, and although the principle is different to slip joints, the length of the lantern fixing is dependent on the nominal diameter of the section in which it is fixed (Standard Norge, 2005d). Part 3-3 of this standard sets requirements for lighting columns as they are to fulfill two limit states, the ultimate limit state (ULS) and the serviceability limit state (SLS). Characteristic loads are calculated in accordance with EN 40-3-1, and should be multiplied with partial load factors, γ_f . Characteristic strength is calculated in accordance with EN 1993-1-1. Bending moments are to be calculated for cross sections at critical positions on the pole. Fatigue is not covered in the standard, but it is stated that fatigue may be considered for poles taller than 9 m.

In NEK EN 50341-1:2012, which is a standard for overhead electrical lines, some requirements for slip joint connections are described. One of the chapters concerns design of support structures, in which steel poles utilizing various connection methods are included. In this standard it is written that EN 1993-1-1 shall be followed unless otherwise stated (Norsk Elektronisk Komite, 2012). However, NEK EN 50341-1:2012 describes that slip joints must be validated by calculation, unless the following observations are fulfilled:

1. *“When modelling the pole considering a global elastic analysis, only the nominal inside male section in the splice area shall be considered for resistance.*
2. *The connections are defined, on drawings, with a nominal lap at least equal to 1,5 times the maximum average diameter across angles of the female section.*
3. *The assembly is carried out on site. To take into account variations in thickness due to the galvanizing and dimensional variations of the polygonal section, the maximum effective length of jointing shall be greater than 1,35 times the maximum average diameter across the angles of the female section.
However, the sum of the slip tolerances at each joint shall comply with the pole length tolerance defined in the NNAs or in the Project Specification.*
4. *The jointing force shall exceed the maximum factored design vertical compressive force at joint level.*
5. *When necessary, anchoring devices on either sides of the slip joint shall be provided on the pole in order to ensure on the site a proper splicing using hydraulic jacks or pulling device according to the supplier recommendations.”*
(Norsk Elektronisk Komite, 2012)

The German National Normative Aspects (NNA) for the 2001 version of the EN 50341-1 standard has been investigated and it stated two additional requirements for slip joint

connections. The first requirement is that pole tapers shall be minimum 10 mm/m. Secondly, the wall thickness shall be maximum 16 mm.

2.4.2 Offshore standards

Even though the slip joint technology only is in the early phase of being applied offshore, its mention in offshore standards have investigated. One of those are the DNV-OS-J101 which is a standard for design of offshore wind turbine structures. The standard has a chapter devoted to design and construction of grouted connections, for wind turbines, but there is no mention of slip joints. Conical grouted connections are described and a recommendation for angles between 1° and 3° is stated (DNV GL, 2014).

A standard for design of steel structures is NORSOK N-004 which describes tubular joints but not types that are relatable to slip joints. There is also a section describing strength of conical transitions (Standards Norway, 2013). These are however not consisting of two segments in contact akin to slip joints.

2.4.3 American standards

A bulletin guide specification for steel transmission poles from 2019 states that design and fabrication should be according to ASCE 48-11, which is a standard for design of steel transmission pole structures. Some requirements regarding the slip joints are stated. Firstly, the structure should have as few joints as possible. The nominal overlap length should be designed as described in the ASCE 48-11 standard (United States Department of Agriculture, 2019). The standard has a subsection devoted to slip joints, in a chapter called “Design of Connections”. Slocum and Fairbairn (2015) have summarized changes in the requirements for slip joint lengths, in the American Society of Civil Engineers (ASCE) standards. Reports by the ASCE, describing the design of steel transmission pole structures, states recommendations for the minimum length of overlap of a slip joint. An ASCE report published in 1978 recommended that a slip joint should have minimum overlapping section that is 1.5 times the inside diameter of the upper section. In a later version (1990) this minimum length was adjusted to 1.35. However, in their publication of 2006, there were no recommended lengths, instead it suggested that splice lengths in the region of 1.42 to 1.52 times the inside diameter of the upper section. The latest ASCE standard, published in 2012, has changed this ratio back to the same recommendation of 1978. The first standard has allegedly test results to back up the recommended length but does not refer to any tests. It may seem that later standard recommendations are based on experience (Slocum and Fairbairn, 2015). A similarity throughout the standards is that overlapping length is defined relative to pole diameter.

2.5 Summary

The slip joint has many advantages over conventional connecting methods. The reported saved time of installation as well as lowered maintenance compared to the alternatives, makes it an enticing solution. It has been in use for many years and recently a motivation to apply the technology offshore has roused. Although the slip joint seems like a viable option for connecting long, slender steel poles, knowledge on its behavior is limited, especially with less than ideal conditions.

In this literature study, some methods for assembling slip joints has been mentioned. Generally, there is desired to perform a controlled assembling procedure, so that a proper fit with required

overlap length is reached and any damage to the structure is avoided. A different approach may be used for installing slip joints for offshore wind turbines than land based light poles. Dropping the upper pole segment has shown to yield insufficient overlap lengths, whereas assembling the slip joint with a hydraulic jack is a proven method. Another method is described, which uses a vibratory device to reach the required overlap. However, this method is not yet in use, and requires further investigation.

Overall there is little description of slip joints in the investigated standards. No mention of slip joints was found in standards for light columns or wind turbines. However, in a standard for overhead electrical lines there is a subchapter stating requirements for slip joints, regarding the overlap length and assembling force.

3 Methodology

3.1 General

The aim of this thesis was to perform finite element modelling and analysis of axial settlement of light poles. The light poles to be studied are of the sort evaluated in the report by DNV GL in 2015, where the slip joint technology is used. The studied phenomenon involves non-linearities and therefore a finite element program called Abaqus has been used. The finite element models of the light poles have been created based on technical drawings of the structures, which were given at the start of the project. The models are simulated with the whole load history from assembling of the slip joint connection, upending of the mast and to being exposed to wind loads. Results from the simulations have been studied with regards to stresses and axial settlement of slip joint connection. Parameter studies have been performed to investigate which parameter could trigger axial settlement at the slip joints.

3.2 Preparatory work

Ahead of the work in Abaqus, there have been conducted some work to identify key parameters for light poles and slip joints. Various parameters such as wall thickness, wind loads, material properties, coefficient of friction and jacking tension during assembly have been investigated and discussed. Through the literature study performed in the beginning of the project, knowledge and awareness of different aspects of the slip joint has been obtained, which have shown helpful in further work. The identification of key parameters for slip joint connections has led to some clarity of which topics that are of interest in the parameter study.

To obtain a more thorough understanding of the slip joint connection, manual calculations have been carried out prior to the simulations and has later been compared with the analyses to evaluate whether the results are reasonable. The calculations have been conducted in PTC Mathcad and involves three different cases: a calculation of friction forces between a mass and an inclined plane, a thick-walled cylinder problem and lastly a computation of radial deflection of a thin cylindrical shell. No directly applicable formulas have been found for the slip joint, and therefore the three calculations that share some similarities with the connection type have been chosen.

3.3 Finite element modelling and analysis

The software that has been used for finite element modelling and analysis is Abaqus, as it supports material non-linearity and contact. Prior to building the full model of the light pole, a smaller and simplified model was analyzed. This model was constructed to only include a slip joint and the nearby region. The model was further simplified by assuming pole sections to be perfectly circular, thus the results could be compared to manual calculations. Also, to lessen the computational effort required, only a quarter of the part, having symmetric boundary conditions, was modelled.

After gaining results and some experience with the simplified model, a more realistic model in terms of geometry and load history, was made. The cross-section of this model was hexadecagonal, to imitate the realistic pole structure. Although the light poles have three slip joints each, their second splice is where significant settlement had been observed and is therefore the only slip joint included in the model. The goal was to establish a load sequence simulating the whole load history from assembling, upending and several years of operation.

The full load history was constructed step by step, making sure each step would work as expected before advancing to the next. Through trial and error, while using the Abaqus User Manual extensively, a suitable load history was obtained. Along the way, complexity was added to the preliminary model. However, the process of creating the load history was not straightforward, e.g. as different analysis types were attempted. Generally, contact in the slip joint seemed to cause much of the difficulties experienced throughout the process of establishing the load history. However, as more experience was gained by the user on how to run simulations, e.g. with contact, such difficulties were resolved. One example of this is that the pre-loading of the slip joint became less problematic to simulate once a controlled displacement step was implemented in advance.

3.3.1 Parameter study

The parameter study was aimed to investigate the effect of varying different parameters related to the slip joint on axial settlement. It includes several analyses in Abaqus where only the parameter to be investigated has been changed from each analysis. The first parameter that has been studied is magnitude of the pre-load. Simulations has been performed with five different pre-load forces: 80 kN, 100 kN, 120 kN, 200 kN and 300 kN which were selected on the basis of the 100 kN pre-loading used in the main simulation. From this pre-load magnitude the other values were selected to be a 20% decrease and 20% increase, but also investigating two significantly increased pre-load forces of 2 and 3 times the magnitude.

The second parameter that has been investigated is the coefficient of friction applied to the contact formulation. There are uncertainties tied to the coefficient of friction and therefore simulations with different values of this parameter has been performed, to investigate its influence on axial settlement. Relatively few simulations have been performed for each parameter, which is explained by the relatively long computational time each simulation requires.

4 Identification of key parameters

There are many parameters for the light poles that potentially could affect the behavior of slip joints. Some of these parameters are related to its geometry, material properties, surface properties and external factors such as environmental loads. In this section the some of the most important parameters thought to affect the extent of axial settlement is considered.

4.1 Overall dimensions

The total pole length may dictate how many slip joint connections are necessary. The previously mentioned light poles, assessed by DNV GL, each had three slip joints as the mast lengths were almost 42 m (DNV GL, 2015). Long poles yield large overturning momentums, which the slip joints must be able to carry. Furthermore, the closer a slip joint is to the bottom of the structure, the more of the structure's self-weight it must be able to carry.

Overlap length is another parameter that affects the slip joints. Longer overlaps imply that larger area theoretically in contact that surface normal forces are distributed over, yielding a smaller surface pressure overall. Therefore, less deformation will appear and consequently less axial settlement. Another parameter that influences the extent of axial settlement is the cone angle. The larger the cone angle is for a slip joint connection the more radial deformation is needed for it to settle axially. On the other hand, a slip joint connection with large cone angle may be more difficult to pre-load sufficiently and obtain a tight connection. There is another important parameter of light poles, namely the wall thickness. Thicker walls mean more material must be deformed in order to accommodate diameter mismatches.

4.2 Dissimilar tapers

Two cones with similar tapers will theoretically fit perfectly together and be in uniform contact throughout. However, in reality this is likely not the case, either due to variations within tolerances or intentionally from the design. Connecting two pole segments with dissimilar cone angles will result in initial contact occurring at one point of the slip joint opposed to uniformly over the whole joint simultaneously. An illustration of slip joint connections with segments of different pole tapers is shown in Fig. 4. Case a) represent equal tapers where the initial contact occurs throughout the whole slip joint. In case b) the top segment has smaller pole taper than the bottom, meaning that initial contact occurs at the bottom of the slip joint. In the last case, c), the top segment has larger pole taper than the bottom, causing initial contact to appear at the top of the slip joint. In the two latter cases, axial settlement must occur before there is full contact throughout the slip joint.

To investigate this topic further, the cone angle of each individual light pole segment has been calculated, based on their technical drawings. The calculation which is to be found in Appendix 1 revealed that one of the mast segments had pole tapers slightly smaller than the others, as listed in Table 1. The slip joint connecting Segment 2 and Segment 3 is therefore similar to case b), although not as severe as shown in Fig. 4.

Table 1 – Calculated pole angles of each pole segment, based on technical drawing dimensions.

Segment	Calculated pole angle
4	0,590
3	0,588
2	0,590
1	0,590

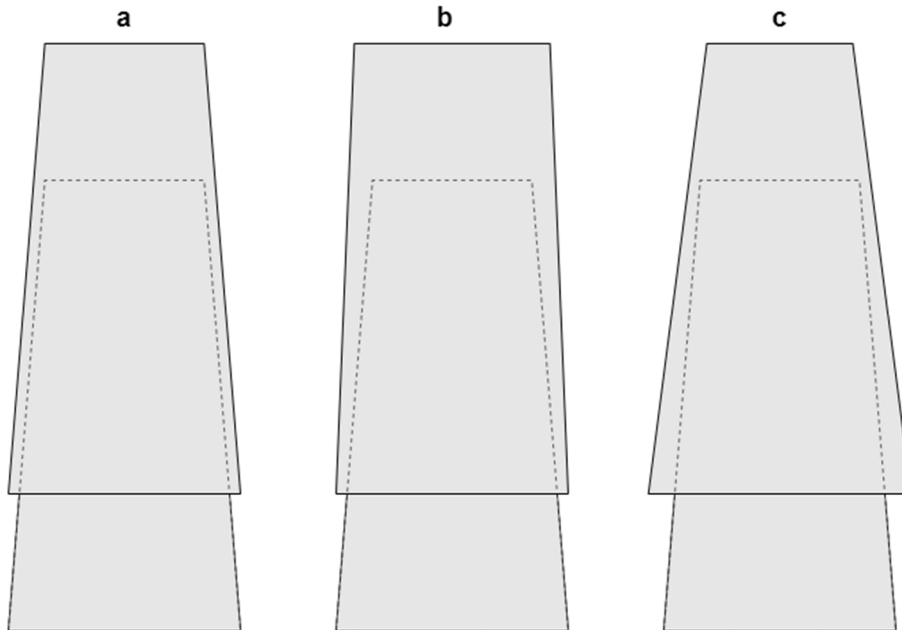


Fig. 4 – Three cases of slip joints with differing pole tapers: a) equal tapers, b) upper pole with smaller taper than the bottom pole and c) upper pole with larger taper than the bottom pole.

4.3 Material properties

The modulus of elasticity, E , is an important material property for slip joint and light pole structures as it is the material's ability to resist elastic deformation. It can be viewed as a stiffness relating imposed stress, σ , to strain, ϵ (Callister JR. and Rethwisch, 2014, p. 214):

$$\sigma = E\epsilon$$

Larger modulus of elasticity gives smaller strains from applied loads. For slip joints, this means that the structure is more reluctant to deforming radially and thus settle axially. However, it also implies that larger jacking tension is required to reach desired overlaps.

A property that is of importance as well is the ductility of the material. Ductility is the amount of plastic deformation has been endured upon fracture (Callister JR. and Rethwisch, 2014, p. 224). Materials with high ductility are called ductile and those with low ductility are called brittle. Slip joints cannot be too brittle, as it undergoes some deformation during assembly, and the joint must not be unnecessarily susceptible to fracture.

4.4 Coefficient of friction

The slip joint connection relies on friction forces which are related to the normal forces by the coefficient of friction (COF). The COF can vary significantly as it is affected by several factors,

such as the materials in contact and their surface properties. Different COF are to be used for static cases and when sliding occurs. Generally, the static COF is significantly larger than the sliding COF, and it is larger for clean surfaces than lubricated ones (Oberg, 2012, p. 166).

The light poles utilizing slip joint technology, evaluated in the DNV GL report, were made of steel but was coated with a protective layer of zinc. In that case it makes sense to use COF for zinc-zinc connections, which is found to be 0.6 (Oberg, 2012, p. 166). Slip joints will necessitate some measure of COF as higher COF means larger friction forces are required for sliding to initiate.

4.5 Orientation of light poles relative to dominant wind direction

The local wind conditions affect the light pole and the slip joint connection. This could include the wind speeds, gusts and dominant wind direction. In the light pole report by DNV GL, two out of four poles had experienced significant ladder deformation (DNV GL, 2015). These two are placed parallel but opposite to each other, with the floodlight array oriented approximately along the same diagonal.

The dominant wind direction could potentially explain why only two of the light poles experienced significant settlement. As seen in Fig. 5, a “wind rose” has been obtained for a nearby location, representing wind data from 2009 to 2015 (Norwegian Meteorological Institute, 2020). The wind rose shows the distribution of winds by their direction, divided into sectors of 30°, and wind speed. Dominant wind directions are found to be from south-south-east (SSE) and the opposite direction, north-north-west (NNW), with considerable winds in neighboring sectors. Generally, the wind speeds are seen to be in the lower regions, from 0.3-5.2 m/s and 5.3-10.2 m/s.

The orientation of the light poles with regards to the dominant wind direction has been evaluated. Fig. 6 shows the location of all four masts, named M1, M2, M3 and M4, with direction of dominant wind indicated by the red arrow. The floodlight arrays can all be thought to face the center of the football pitch, although likely with some deviation. Masts M1 and M2 have practically equal but opposite angles of orientation relative to the dominant directions of wind. Therefore, it is difficult to conclude whether the wind loads have had different impact on each of the light poles.

Wind rose, frequency distribution of wind

Wind direction divided in sectors of 30°

Frequency distribution of wind speed in percent %

Wind speed (m/s)

- > 20.2
- 15.3-20.2
- 10.3-15.2
- 5.3-10.2
- 0.3-5.2

Calm (%)



Year: 2009 - 2015

Jan, Feb, Mar, Apr, May, Jun, Jul, Aug, Sep, Oct, Nov, Dec

Hour: 0, 1, 2, 3, 4, 5, 6, 7, 8, 9, 10, 11, 12, 13, 14, 15, 16, 17, 18, 19, 20, 21, 22, 23 (NMT)

44560 SOLA

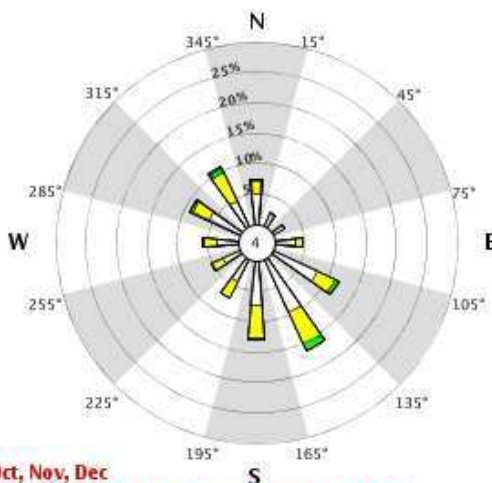


Fig. 5 – Wind rose of collected wind data from 2009-2015, from a nearby station (Sola). Obtained from Norwegian Meteorological Institute (Norwegian Meteorological Institute, 2020).



Fig. 6 – Principal dominant wind direction, SSE, at site, with the four masts denoted M1, M2, M3 and M4.

4.6 Effect of temperature

Variations of temperature is something that can affect the extent of axial settlement experienced in a slip joint. It is well known that metals expand upon heating. In emergence of warm weather, the outer segment of the slip joint could potentially heat up and expand radially slightly faster than the inner segment. In that situation, some decrease in interfacial pressure between the segments can be expected, making the slip joint more susceptible to axial settlement.

4.7 Jacking tension during assembling

When assembling with hydraulic jacks, the amount of jacking tension applied determines how tightly the pole segments are fitted together. In this procedure, hydraulic jacks essentially pull one segment over the other with certain forces. The required force to continue to pull the segments further together will increase as the process goes on, due to increasing difference between the nominal diameters of the segments. Applying more jacking tension to a slip joint will increase the surface pressure between the segments, essentially creating a more rigid joint, and it will also slightly increase the joint contact surface as the overlap length increases. The slip joint will likely experience less axial settlement during operation when it has been properly pre-tensioned, however this issue is investigated later in the thesis. Equal jacking tension from all jacks should be a requisite, as asymmetrical joining may cause non-uniform contact around the cross-section of the slip joint.

4.8 Misalignment of cross-sections during assembling

When assembling slip joints of structural poles with polygonal shapes, consideration must be put into the alignment of their cross-sections. Theoretically, if the their cross-sections do not match, meaning that one segment is rotated slightly relative to the other, there will initially be a loss of contact in the connection, as depicted by the colored area in Fig. 7. The loss of contact implies the appearance of altered stresses in certain areas, due to the small contact surfaces. Surfaces in contact will deform, either plastically or elastically, so that finite areas of contact are formed (Fenner, 1986, p. 213-236). The resulting deformed cross-section can have reduced carrying capabilities. It is reasonable to expect larger axial settlements of a slip joint where loss of contact due to misalignment of cross-sections is appearing. This is because of the decrease of total surface area that must be able to carry the same magnitude of loads, resulting in higher local stresses. The discussed matter is not a problem for a perfectly circular cross-section. The extent of the worst possible misalignment for hexadecagonal sections is also limited due to its shape being relatively close to circular. Gaps can however form due to geometric variations within fabrication tolerances, and the same problem occurs.

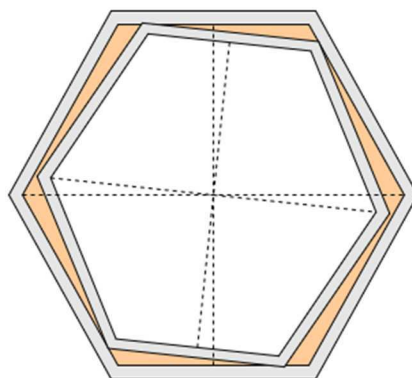


Fig. 7 – Misalignment of two hexagonal cross-section causing gaps (orange area) and loss of contact.

5 Manual calculations

5.1 Purpose of the manual calculations

The manual calculations were intended to serve as theoretic background and a foundation for interpreting the finite element simulations. Three different cases were investigated and is described in the current chapter. First a two-dimensional problem of a body on an inclined plane was studied. By performing this computation, an idea of friction forces acting in the slip joint has been obtained. The second computation concerns a thick-walled cylinder compound, where interfacial pressure was among the studied effects. Lastly, formulas for thin-walled cylindrical shells under axisymmetric loading were used to calculate and plot the radial deflection of a cylindrical shell segment. All the manual calculations have been carried out in PTC Mathcad and can be found in Appendix 2, Appendix 3 and Appendix 4 respectively.

5.2 Case 1: Friction between a body and inclined plane

The first manual calculation, shown in Appendix 2, is a two-dimensional problem where a body with mass is placed on an inclined plane. The mass was thought to represent the combined weight of all elements carried by the second slip joint, which is 4856 kg. For slip joints the cone angle is relatively small, and in the calculation, it was set to just 0.59° , yielding a plane inclination angle of 89.41° from the horizontal axis. The friction force acting between the body and the inclined plane, F_{fr} , was calculated according to the formula for friction:

$$F_{fr} = \mu N \quad (1)$$

where μ is the coefficient of friction and N is the normal force acting between the body and the plane. The coefficient of friction was determined to be equal to the coefficient of static friction for a clean zinc-zinc connection. In the Machinery's Handbook this value is stated to be 0.6 (Oberg, 2012, p.165-166). The Normal force, N , stems from the vertical gravitational force from the mass. Decomposition of the gravitational force in the direction of sliding, G_s , and normal to the sliding surface, G_N , is shown in Fig. 8. G_N is equal but oppositely directed to the normal force acting on the body.

Due to the small cone angle, F_{fr} was calculated to be just 294 N. This value is much smaller than the value of G_s , meaning that the effect of friction alone is not sufficient to hinder sliding. The reason for this is the very high inclination angle. However, the angle at which the friction forces are sufficient to barely hinder slip is termed the angle of repose and can be calculated from (Oberg, 2012):

$$\theta_{repose} = \tan^{-1}(\mu) \quad (2)$$

This formula implies that the angle of repose solely depends on the coefficient of friction. For $\mu=0.6$, the angle of repose is just below 31° measured from the horizontal axis. Regarding the slip joint connection, this is not a practically viable solution. Instead, there must be other effects resisting the relative axial sliding of mast segments in the slip joint connection.

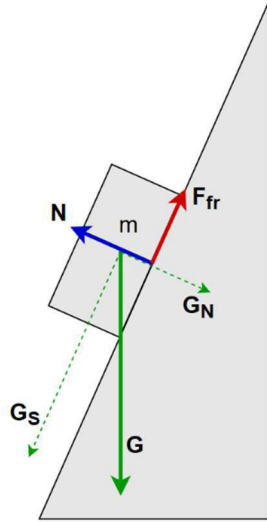


Fig. 8 – Case 1: Mass on inclined plane with friction forces. Gravitational force is decomposed in the direction of sliding and normal to the plane.

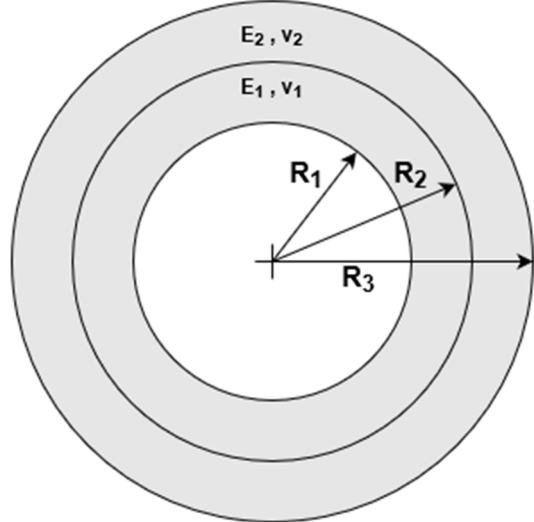


Fig. 9 – Illustration of a thick-walled compound cylinder cross-section.

5.3 Case 2: Compound cylinder

5.3.1 Theory

As the two pole segments of a slip joint are forced together, a mismatch between diameters appears due to the conical shape of the poles. This type of connection is relatable to compound cylinders with interference fits, meaning that the nominal diameter of the inner cylinder is slightly larger than the nominal diameter of the outer cylinder. The theory for such connections is well known in engineering. The calculation described in this section is found in Appendix 3.

To apply formulas for compound cylinders to the slip joint, some assumptions must be made. First of all, the cross section of the slip joint must be assumed to be perfectly circular, as it in reality is hexadecagonal. The hexadecagon is however not very dissimilar to a circle. Secondly, the slip joint must be assumed to be a thick-walled cylinder. Generally, cylinders where the ratio of radius to wall thickness is smaller than 10 ($R/t < 10$) must be considered thick-walled. This is because hoop stresses are not uniform throughout the thickness, and radial stresses cannot be neglected (Young et al., 2011). Lastly, the elastic properties are assumed to be equal for the two separate cylinder parts.

From the calculation of friction, required force to avoid sliding was found and thus, the necessary normal force. This normal force can be converted into a surface pressure by dividing by the total slip joint area, assuming that the normal forces are evenly distributed throughout the connection. The mismatch, δ , between nominal radii of the components has been found from the following formula where the elastic properties of the material is assumed to be similar for both components (Fenner, 1986, p.173-174):

$$\frac{2P(K_1^2 * K_2^2 - 1)}{E(K_1^2 - 1)(K_2^2 - 1)} = \frac{\delta}{R_2} \quad (3)$$

where P is the interfacial pressure, and K_1 and K_2 are ratios of radii R_2 to R_1 and R_3 to R_2 respectively. The stresses in each cylinder component can be calculated from:

$$\sigma_{rr_1} = -\frac{P}{K_1^2 - 1} \left(K_1^2 - \frac{R_2^2}{r^2} \right) \quad (4)$$

$$\sigma_{\theta\theta_1} = -\frac{P}{K_1^2 - 1} \left(K_1^2 + \frac{R_2^2}{r^2} \right) \quad (5)$$

$$\sigma_{rr_2} = \frac{P}{K_2^2 - 1} \left(1 - \frac{R_3^2}{r^2} \right) \quad (6)$$

$$\sigma_{\theta\theta_2} = \frac{P}{K_2^2 - 1} \left(1 + \frac{R_3^2}{r^2} \right) \quad (7)$$

where σ_{rr_1} and σ_{rr_2} are the radial stresses for the inner and outer cylinder component respectively. Similarly, $\sigma_{\theta\theta_1}$ and $\sigma_{\theta\theta_2}$ are respective hoop stresses of the inner and outer cylinders. Throughout the calculations, ratio K_1 and K_2 are assumed to be constant, based on the fact that the pole taper is small, and thus very large axial settlement must occur before these ratios change significantly.

5.3.2 Calculating axial movement as a result of assembling

At initial contact between the two pole segments, there is no surface pressure between the segments as there is no mismatch of radii. Due to the conical shape of the poles, the mismatch increases as the components are pulled further together. As mentioned in the literature study, the force used to assemble the slip joint shall exceed the vertical compressive force that appears once the pole has been upended. From the calculation of friction, the gravitational force was found to be approximately 47,640 N. Therefore, an assembly force, $F_{assembly}$, exceeding this value multiplied by a factor of 2 is selected in the following calculation:

$$F_{assembly} = 100000 \text{ N}$$

In the formula for thick walled compound cylinders, the surface pressure, P , can be replaced by normal force divided by contact area, while the normal force can be replaced by friction force divided by coefficient of friction.

$$P = \frac{N}{A} = \frac{F_{fr}}{\mu A} \quad (8)$$

where N is the normal force, A is the total slip joint contact surface area, F_{fr} is the friction force and μ is the coefficient of friction. Replacing the surface pressure in the thick-walled compound cylinder, yields:

$$\delta = \frac{2R_2(K_1^2 * K_2^2 - 1)}{E(K_1^2 - 1)(K_2^2 - 1)} * \frac{F_{fr}}{\mu A} \quad (9)$$

Sliding during assembling will stop once friction forces are equal to the applied force component in direction of sliding, $F_{fr} = F_{assembly} * \sin(\theta)$. The value of δ has been calculated, which for total assembling force of 100,000 N was found to be 0.012 mm. This amount of mismatch corresponds to a settlement that can be calculated. The pole segments have tapers of 20 mm/m, meaning that the pole diameters decrease at a rate of 20 mm per meter throughout its length. δ which concerns the radial mismatch, is related to the axial settlement through:

$$\frac{taper}{2} = 0.01 = \frac{\delta}{s} \rightarrow s = 100\delta$$

The calculated displacement from assembling is found to be 1.164 mm, which is small compared to observed settlements. Hoop stresses in both cylinders are low for this amount of mismatch, and the radial stresses are negligibly small in comparison.

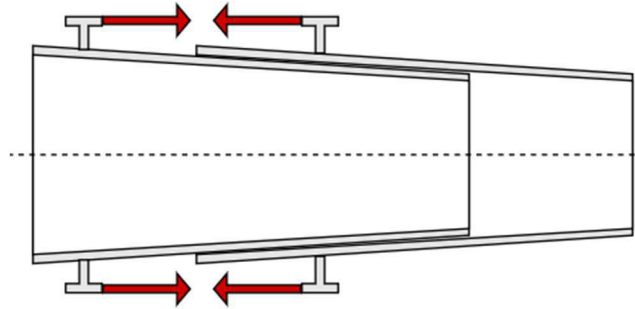


Fig. 10 – Illustration of applied forces during horizontal assembling of a slip joint.

5.3.3 Calculating for a more significant axial displacement

There is of interest to investigate a case where more significant axial settlements have occurred. In the report by DNV GL, one of the slip joints were described to have settled 26 mm. The following calculation uses this value to find hoop stress and check the friction force.

A settlement of 26 mm corresponds to a change in radial mismatch of 0.260 mm. Assuming that the slip joint has been assembled such as in Subsection 5.3.2 before axial settlement occurs, the total mismatch becomes 0.272 mm. Hoop stresses for this mismatch is found to be -47.99 MPa for the inner cylinder meaning that it is in compression. The hoop stress in the outer cylinder, being in tension, is computed to 64.87 MPa. The interfacial pressure at 26 mm settlement is computed to be 0.77 MPa. This can be converted into friction forces by the following computation:

$$F = \mu N = \mu PA$$

The resulting friction force is found to far exceed the gravitational force component in the direction of sliding. This implies that there must have been other effects assisting the self-weight of the structure to obtain such extents of axial settlement.

5.4 Case 3: Thin-walled cylindrical shell under axisymmetric loading

In this calculation, formulas for long, thin-walled cylindrical shells have been used to find the radial deflection during axisymmetric loading. These formulas were found in Roark's Formulas for Stress and Strain (Young et al., 2011). A load case in which similarities can be drawn to the slip joint connection has been found, shown in Fig. 13. This calculation is applicable for long, cylindrical shells with the left end free, and a uniform radial pressure applied near the right end. The formula for radial deflection, y , is stated as follows:

$$y = y_A F_1 + \frac{\psi_A}{2\lambda} F_2 + L T_y \quad (10)$$

where y_A and ψ_A are the radial deflection and the meridional slope, respectively, at the free end.

$$y_A = -\frac{q}{2D\lambda^4} (B_2 - A_2) \quad (11)$$

$$\psi_A = -\frac{q}{D\lambda^3} (B_3 - A_3) \quad (12)$$

LT_y is a load term for the selected load case. F1 and F2 are hyperbolic functions of λ and x , where x is the distance from the start of the shell and λ is a constant:

$$\lambda = \left[\frac{3(1-\nu)^2}{R^2 t^2} \right]^{\frac{1}{4}} \quad (13)$$

The calculation, found in Appendix 4, does however not work well with loads applied less than $6/\lambda$ from the right end. This ratio was calculated to approximately 250 mm. Dimensions selected for the shell is based on the dimensions for one of the actual pole segments. The full length of the selected segment is 11,100 mm with a radius of approximately 500 mm and a thickness of 6 mm. The length of the uniform radial pressure is set to 1600 mm similar to the slip joint. In the calculation, the radial pressure that is used is the value that is found in the previous manual calculation case, i.e. 0.77 MPa. The radial deflection has been calculated and plotted for values close to the end, as shown in Fig. 11. Too close to the end, the radial deflection values deviate severely and are not plotted. The radial deflection is found to be equal throughout much of the length at where uniform pressure is applied. There is little radial deflection away from the region where pressure is applied.



Fig. 11 – Plotted radial deflection, 9000 mm from the free end to the end of the segment (11,100 mm).

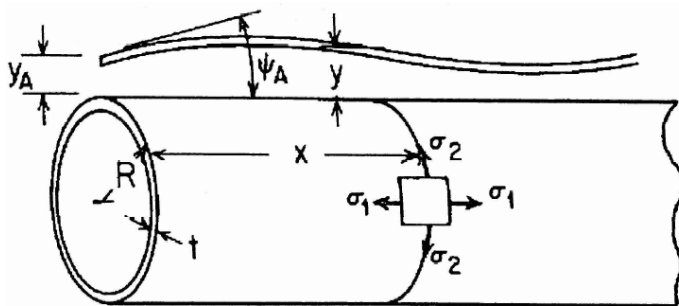


Fig. 12 – Long, thin shell with left end free and right end more than $6/\lambda$ from the closest load. Radial deflection of the shell at any point along the length of the shell indicated by y (Young et al., 2011).

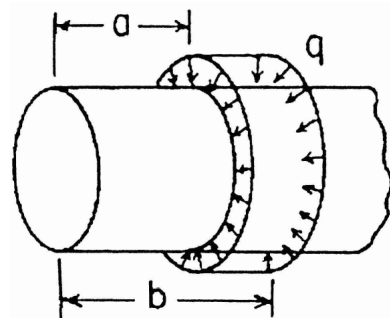


Fig. 13 – Load case: Uniform radial pressure from a to b (Young et al., 2011).

6 Finite Element Modelling and Analysis

6.1 Introduction

In this chapter the central aspects of the finite element modelling and simulation of light poles are described. Firstly, the actual pole geometries are briefly described, followed by a description of the loading procedure from assembling to several years of operation. A material definition has been made. To analyze behavior of the slip joint connection two models has been made; a simplified slip joint model, and more realistic model. The simplified model was purposed to give a basis for the more realistic and complex simulations and has been compared to the manual calculations previously described. The realistic model has been created with more accurate geometry and is subjected to the full loading procedure.

The program used for finite element modelling and analysis is Abaqus. All simulations have been calculated with the Standard implicit solver, which is suitable for static and dynamic low-speed simulations (Simuleon, n.d.).

6.2 A brief description of the masts

The inspected light poles are over 47 m tall and consist of five pole segments. The bottom four pole segments are all between 11 and 12 m long, are connected in series by use of the slip joint technology, forming a mast approximately 42 m long. On top of this mast, the fifth segment is connected which acts as an attachment pole for the floodlight array. There are also two service platforms mounted to the pole, one at the top of the mast and one partway up the pole length. A ladder, at where axial settlement was observed, is attached with brackets along the length of the mast so that service platforms can be accessed during inspection or maintenance. A drawing of the full light pole assembly is shown in Fig. 14, indicating segment numbers and including nominal length of segments as well as overlapping regions.

The cross-sectional profiles are hexadecagonal, i.e. having the shape of a 16-sided polygon. This shape is shown in Fig. 15, where the sides are numbered, indicating that there is a total of 16 sides. Along the lengths of the pole segments there are two longitudinal welds. All of the pole segments are tapered, meaning that their bottom diameter is larger than their top diameter, thus having conical shapes. This conical shape is an essential characteristic to be able to use the slip joint technology. Three slip joints are used to assemble the four pole segments together. The nominal length of the slip joints, i.e. the nominal length of the overlapping region, range between 1.5 m and 1.9 m. Approximately 4900 kg rests on the second slip joint, while the mass of the whole structure is around 12,400 kg.

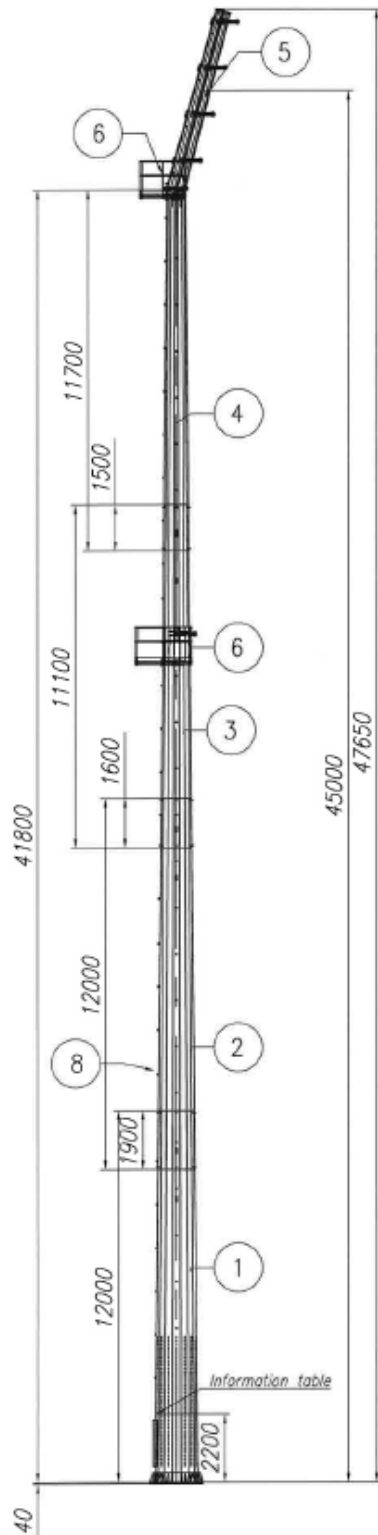


Fig. 14 – Technical drawing of lighting mast, with some dimensions in mm. Length of overlapping sections is also shown. Numbers 1-4 indicate the corresponding segments, 5 indicates the flood light array, 6 is two service platforms and 8 indicate placement of attached ladder (Technical drawings).

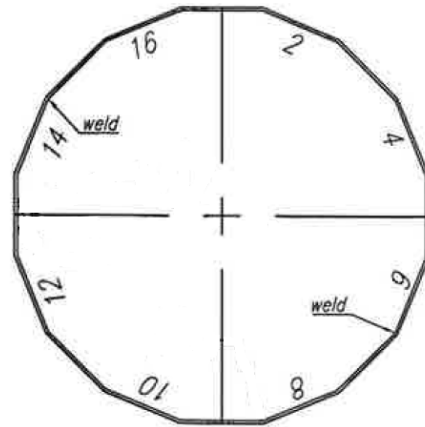


Fig. 15 – Cross-section of pole segment. Numbers indicate the side numbers. Longitudinal welds are located (Technical drawings).

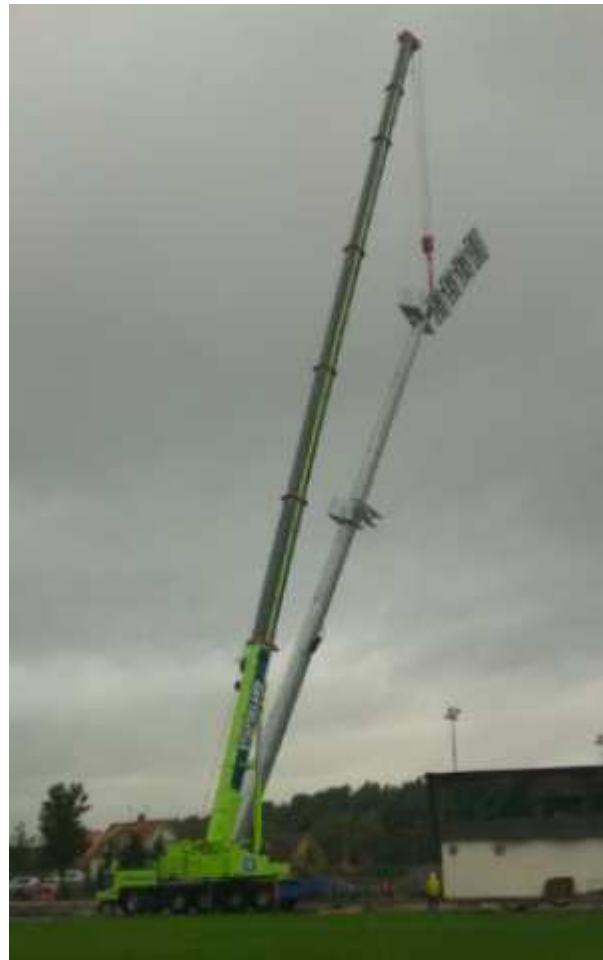


Fig. 16 – Picture of the assembled floodlight pole, during upending procedure (DNV GL, 2015).

6.3 Loading procedure

This section gives an overview of the general loading procedure that the floodlight mast undergoes during simulation. The procedure of loading that has been applied to the finite element model was aimed to reflect the load history, from assembling to several years of operation. It is possible to divide this loading procedure into three main parts:

1. Pre-load
2. Upending
3. Wind loads

Although there are three main parts, more steps have defined in the finite element model to describe the loading procedure. However, the stepwise inclusion of loads and boundary conditions are further described later in this chapter.

6.3.1 Pre-loading

As previously mentioned in the literature study, there are various ways of assembling slip joints, one of which is pre-loading with the use of hydraulic jacks. Essentially two hydraulic jacks are attached to the handles, while the mast lays horizontally. Prior to the pre-loading there is assumed to be no contact pressure between the segments. As the hydraulic jacks are pressing the slip joint together with oppositely directed forces a surface pressure is bound to appear between the segments.

The compressive pre-loading force that has been applied for the actual masts is unknown, but suggestions found in the previously discussed standard can be used as a basis for estimating the pre-load force magnitude. NEK EN 50341-1:2012 states that “The jointing force shall exceed the maximum factored design vertical compressive force at joint level.” (Norsk Elektronisk Komite, 2012). Therefore, the vertical compressive force, caused by the weight of all structural elements placed on top of the slip joint, have been calculated. The combined weight resting on the second slip joint is found to be approximately 4900 kg based on numbers given in the technical drawings. This mass multiplied by the gravitational constant yields a vertical compressive force of 48 kN, which again is multiplied by a factor of 2 to find a suitable estimate for the pre-load force. The selected pre-load force, used in the analyses, is 100 kN. This is the total force, meaning that when two hydraulic jacks are used, each jack pull with a force of 50 kN. The pre-load force is also a subject of investigation in the parameter study described in Section 7.4.

6.3.2 Upending

After the slip joints have been pre-loaded and all other components are attached to the mast, the structure is due for upending. A crane is lifting the very top of the mast structure so that it is rotated 90°, from laying horizontally on the ground to standing vertically. Once the mast has been upended, its bottom end is bolted to the foundation. Fig. 16 shows the actual mast during the upending procedure.

6.3.3 Wind loads

6.3.3.1 General

Once the mast has been upended, it is subjected to wind loads. Through several years of operation, the mast has been exposed to winds from various directions with different magnitudes. Through the many years of operation, the winds have caused varying responses in the structure, e.g. due to different wind patterns. Although the small lateral oscillations may

slowly have contributed to the axial settlement in the slip joint connection, the simulations have been solely concerned with a series of large storms.

The current subsection concerns the modelling of a suitable wind model that has been used in the finite element analysis. First some of the general considerations when modelling wind is discussed, then a description of the wind load distribution along the mast is described followed by the modelled wind history.

6.3.3.2 Effects of the wind

There are a lot of uncertainties related to the wind as it varies in velocity, direction and oscillates in a random and unpredictable manner. Wind generally moves horizontally due to differences in air pressure but can also have a vertical component. The wind speed is often defined in terms of the average wind speed over 10 minutes. Another important parameter of the wind is gusts, i.e. the maximum average wind speed over 3 s (Store Norske Leksikon, 2019). A gust is a sudden increase in wind speed, which can be potentially harmful to a structure.

Wind forces can have different effects on a structure. For a tall structure, such as a light pole, the wind causes bending similar as for a cantilever beam. Bending of such a structure, attached at one end, imply that the maximum deflection is at its very top. The magnitude of deflection cannot be too large, as it may damage partitions in the structure (Encyclopædia Britannica, 2020).

Another effect of the wind is sideways swaying caused by flow of wind past a structure, where wind pressure is changing due to unstable vortices (Encyclopædia Britannica, 2020). The wind can therefore cause vibrations in a structure where its periodic motion is perpendicular to the direction of the wind. How the wind affects a structure, may depend on its natural frequency. If the natural frequency of the structure matches the frequency of applied forces, resonance occurs which yield large deflections (Rao, 2017, p.39).

A frequency analysis has been performed for the mast model, after it has been pre-loaded and upended. From the frequency analysis the natural frequency of the model was found to be 0.59 Hz. According to NORSOK N-003, a standard for actions and action effects for offshore structures, a structure with eigenfrequency less than 5 Hz are considered dynamically sensitive. Structures that are dynamically sensitive must be considered for dynamic effects. High towers are among the typical structures for which dynamic effects shall be considered (Standards Norway, 2017). Although an offshore standard may not be directly applicable to light poles using slip joints, it may give be suggestive of important aspects in some cases.

6.3.3.3 Wind load distribution

The wind has been thought to be acting horizontally on the mast structure. Wind speeds vary with the elevation; thus, the wind pressure varies along the length of the light pole. At the same time, the pole diameter decreases with height, meaning smaller wind area at where the wind pressures act.

To establish a suitable wind distribution along the length of the mast, a previous calculation of wind forces for the current light poles, has been used. The calculation can be found in Appendix 5, where the wind force has been calculated for several positions along the height of the model and is expressed in terms of a line load in the longitudinal direction of the mast. Calculated values of wind force per meter is represented by the blue line in Fig. 17. Throughout large portions of the light pole, wind loads are relatively similar. The only significant increase in

wind loads is at the very top, due to the floodlight array and the big platform, as well as at the small platform about 27 m from the bottom.

For simplicity, the wind loads have been assumed to be uniformly distributed over the regions which they are applied. In the finite element model, the wind line load has been defined with different magnitude for three different regions, namely the bottom beam, the top beam of the mast and the beam at where floodlights are attached. To transform the calculated wind loads into uniform line loads for the three different regions, the sum of moments has been calculated. The sum of moments from line loads acting over the region which they are representing, divided by the length of the region times the average moment arm, has been used to find an equivalent uniform line load for each region. Thus, the overturning moment should be exactly similar for the model as in the calculation. The resulting uniform line loads are plotted in Fig. 17 represented by red lines, along with the calculated values coloured blue.

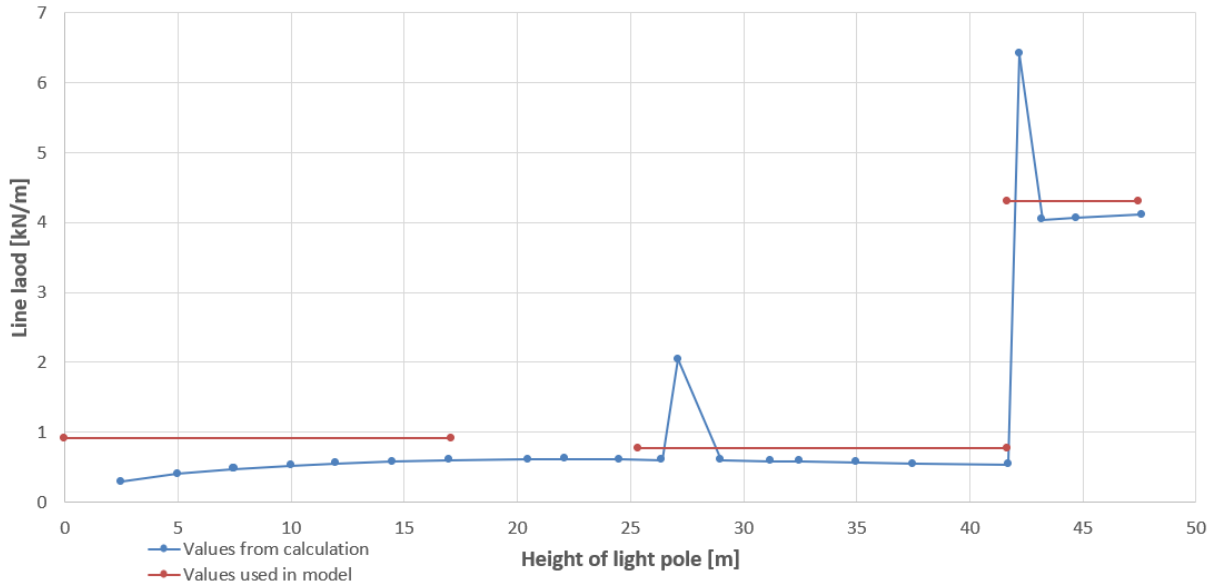


Fig. 17 – Plotted values of wind force per meter. Blue line represents the calculated wind line loads, whereas the red line represents the simplified line load applied to the finite element model.

6.3.3.4 Wind history

Over the years of operation there are various winds that has various effects on the structure. A wind load history has been established that represents a series of heavy storms, in which winds from different directions has been included. Therefore, the dynamic part of the wind model works as a scaling in magnitude of the wind distribution with respect to time. The wind model concerns the large changes in wind and does not include the high-frequency oscillations.

The wind history represents a total of five storms. Each storm has been modelled to be ramped up to its peak value and subsequently oscillate $\pm 15\%$ around its average wind speed for eight periods, before being calmed down. The series of storms is to be seen in Fig. 18.

The first storm acts in the positive z-direction with a scaling factor of 1, followed by a second storm in the same direction but a scaling factor of 1.5. The third storm acts in the positive-x direction with a magnitude of 1, followed by a storm of magnitude 1.5 in the negative x-direction. The last storm has components in the positive z-direction and the negative z-direction, each of magnitude $1.5/\sqrt{2}$, which sums up to a total magnitude of 1.5.

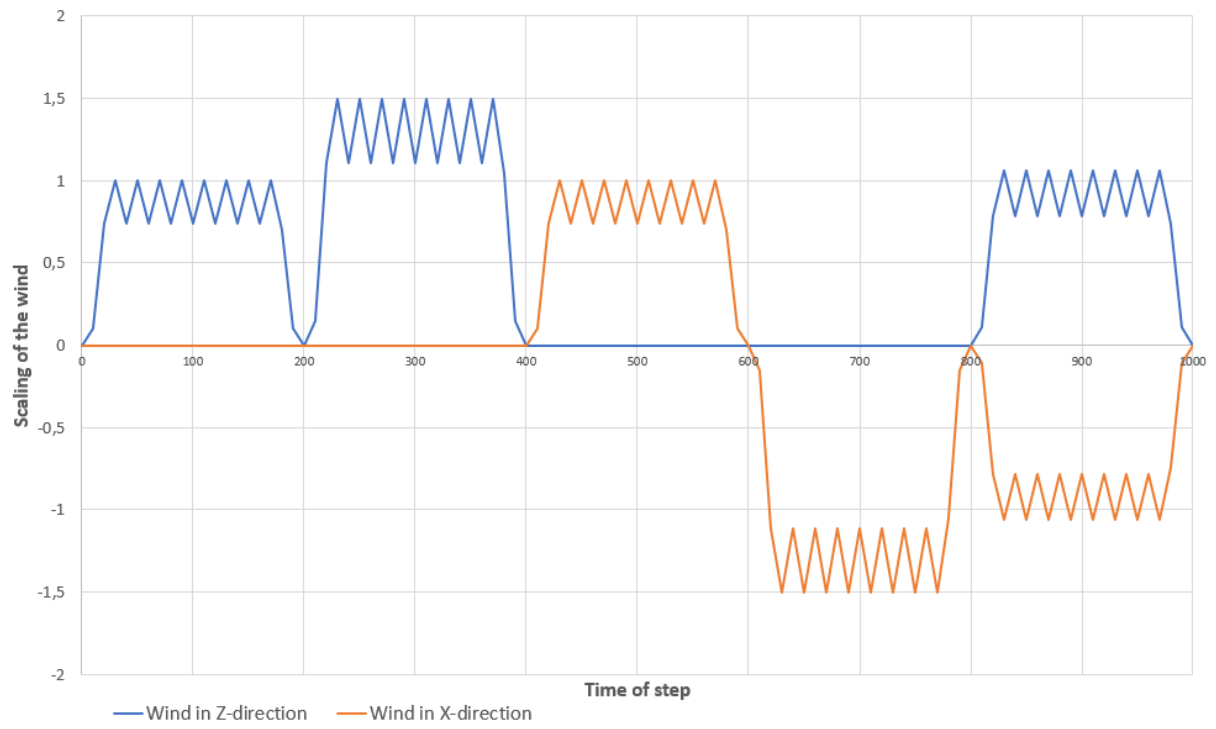


Fig. 18 – Scaling of wind loads creating a series of five large storms, in z-direction (blue) and x-direction (orange).

6.4 Material definition

Prior to performing the finite element simulations, the material properties have been defined for the model. It includes definitions for elasticity, plasticity and density. All sections of the model have been assigned the same material, meaning only one material model has been defined. Throughout this section the process of defining material is described.

6.4.1 Elasticity and plasticity

According to the technical drawings, the floodlight masts are made of structural steel S355J2. In order to obtain appropriate stress-strain data for this material, a Recommended Practice (RP) made for determination of structural capacity by non-linear finite element analysis methods (DNV GL, 2019) was used. In the RP there is stated that the material curve should be modelled being stepwise linear and use a power law, as well as having a yield plateau, as can be seen in Fig. 19. Properties for S355 steels are proposed in the RP, as tabulated in Table 2. Listed are the Young's modulus, E , stress-strain curve parameters σ and ε , the Ramberg-Osgood parameter K and factor n . The tabulated values are valid for thicknesses up to 16 mm. The stress-strain curve parameters are indicated in Fig. 19. The figure also indicates the stepwise linear section (Part 1 and Part 2), the yield plateau (Part 3) and the power law region (Part 4).

The Young's modulus of 210,000 MPa and Poisson's ratio, ν , set to 0.3, together comprise the elastic properties of the material defined for the finite element model. The stress-strain curve in the region of the yield plateau is plotted based on the stress-strain curve parameters given in Table 2. Material behavior for stresses past the second yield point has been modelled with use of the following Equation to obtain stress strain values:

$$\sigma = K \left(\varepsilon_p + \left(\frac{\sigma_{yield2}}{K} \right)^{\frac{1}{n}} - \varepsilon_{p,y2} \right)^n \quad \text{for } \varepsilon_p > \varepsilon_{p,y2} \quad (14)$$

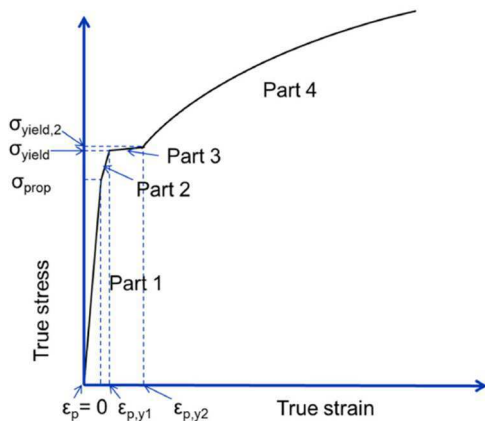


Fig. 19 – Definition of stress-strain curve, indicating stress-strain curve parameters. (DNV GL, 2019).

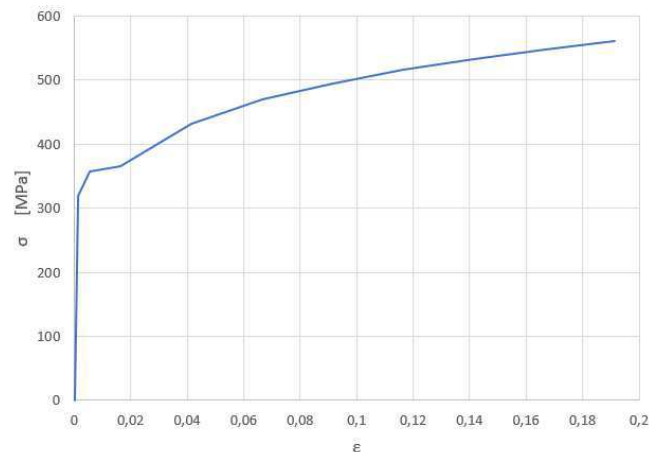


Fig. 20 – Plotted stress-strain curve for S355 structural steel, for strains up to 0.19.

Table 2 – Properties for S355 steels (true stress strain) proposed by DNVGL-RP-C208 (DNV GL, 2019)

S355	
Thickness $t \leq 16$ mm	
E [MPa]	210000
σ_{prop} [MPa]	320.0
σ_{yield} [MPa]	357.0
σ_{yield2} [MPa]	366.1
ϵ_{p_y1}	0.004
ϵ_{p_y2}	0.015
K [MPa]	740
n	0.166

Table 3 – Given and calculated corresponding stress-strain values used to define plastic behavior of the finite element model

σ [MPa]	ϵ_p
320.0	0
357.0	0.004
366.1	0.015
399.6	0.025
423.0	0.035
441.3	0.045
456.4	0.055
495.6	0.090
527.0	0.130
556.4	0.180

Stresses has been calculated for seven values of plastic strain, ϵ_p , in an Excel sheet. Thus, a total of ten points have been used to determine the plastic material behaviour for the finite element model in Abaqus. The calculated values for stresses and the corresponding plastic strains are given in Table 3, along with the given values from Table 2. The resulting stress-strain curve has been plotted and is shown in Fig. 20.

6.4.2 Density

The density of the material has been defined, as it is needed in Abaqus/Standard for simulations involving gravity and in dynamic analyses. According to Eurocode 1, the density of steel varies from 7700 to 7850 kg/m³ (Standard Norge, 2019). The typical density of structural steel for structural design is 7850 kg/m³ (Eurocode Applied, 2009) and therefore this value has been assigned to the material model.

6.5 Simple model

6.5.1 General

Prior to working with the main model, a simpler model has been created. It is simpler in the way that its geometry does not fully reflect the actual mast. Also, the whole load history that the light poles undergoes has not been applied to this model. This model only concerns pushing one segment over the other. Due to the symmetric geometry and loading applied, only one quarter of the cross-section has been modelled, to reduce the required computational time. During this section describing the simplified model, some aspects are discussed only briefly such as element type and contact formulation, as it is discussed further when the main model is described.

6.5.2 Geometry

The geometry of the simplified model has been constructed with some assumptions in mind. Firstly, the cross-section profile for the model differs from the actual profiles in that they are circular opposed to sixteen-sided. The circular cross-section profile made the results from the current model more comparable to the manual calculations performed in the previous chapter, than if it were to be modelled with hexadecagonal cross-section. The second assumption is that the pole tapers are equal for the two segments in contact, thus forming a more uniform contact pressure. Again, this assumption was intended to make the analysis results comparable to the manual calculations.

Only regions of the pole segments near one of the slip joint connections have been modelled, as deformations in the slip joint connection has been assumed to have little to no influence on material far from the joint. Therefore, the length of each segment was set to 5000 mm. Dimensions used for modelling the two segments were based on the technical drawings for the actual light poles. The slip joint that has been analyzed in this section is the middle one, i.e. the slip joint connecting Segment 2 and Segment 3. Thicknesses of these pole segments are 8 mm and 6 mm respectively. The two segments were assembled with an overlap but no initial contact, meaning that there was a very small radial gap prior to analyses.

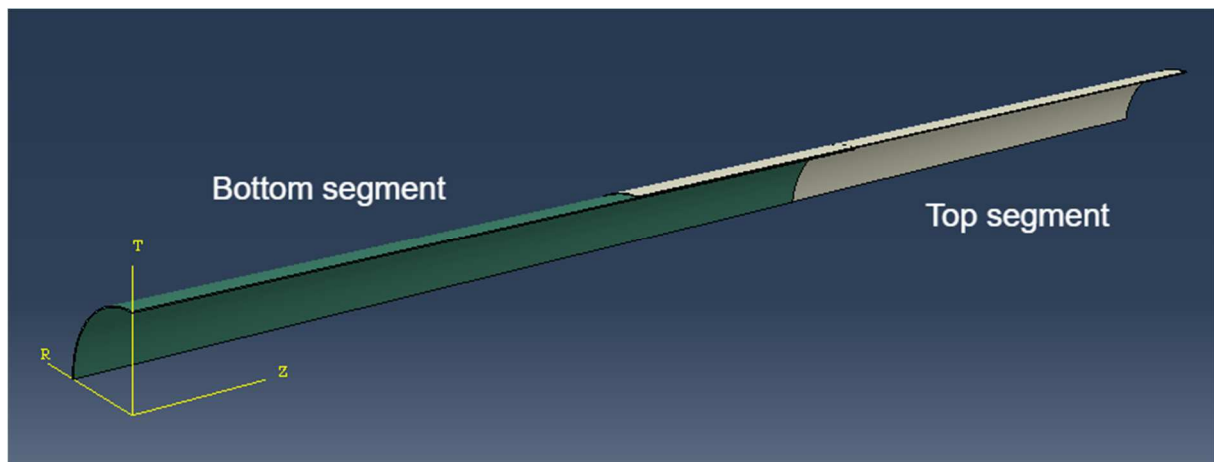


Fig. 21 – Undeformed simple model of the slip joint connection. Bottom segment colored green and the top segment is colored white. Assembled with overlap but no contact prior to analyses.

6.5.3 Mesh and element type

Both parts of the assembly have been assigned a continuum shell element type named SC8R, which is an 8-node quadrilateral in-plane element with reduced integration and hourglass control for general purpose. The parts have been meshed with only one element through their thickness and fifty elements along the circumference of the segments, which was sufficiently to describe the circular shape of the profile. A region of one meshed segment is shown in Fig. 22.

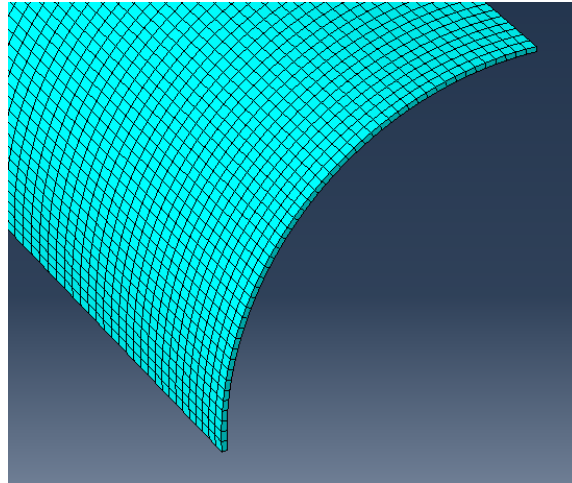


Fig. 22 – Mesh applied to one of the segments of the simplified model.

6.5.4 Boundary conditions

The simulation procedure for this model consisted of only one step, where the two segments were pressed together. To facilitate the assembling of the two segments, the region of the bottom segment was fixed in all degrees of freedoms at its very bottom surface. At the top surface of the top segment an axial displacement is applied through the analysis step. Two simulations have been performed for two different displacement values. The first displacement was set to 5 mm which corresponds to roughly 1 mm of axial settlement past initial contact. The second displacement value was set to 30 mm, which after obtaining contact between the two segments, corresponds to circa 26 mm of settlement.

Along the lengths of the segments symmetry boundary conditions have been applied so that symmetry of the model about the YZ- and XZ-planes have been obtained. Thus, the cross-section is in practice fully circular but only one quarter of it was involved in the calculations.

6.5.5 Contact formulation

The contact formulation for the simplified model is only discussed briefly in this subsection. A similar interaction property is used for the more realistic model and will be discussed in further detail in Subsection 6.6.5. However, the interaction property is defined in terms of a normal and a tangential behavior. The normal contact behavior is set to “Hard” contact, and the surfaces in contact are allowed to separate after contact. The tangential behavior uses penalty-based friction with a coefficient of friction set to 0.6.

A surface-to-surface contact formulation has been used between the two segments. The outer surface of Segment 2 is defined as the master surface, while the inner surface of Segment 3 is defined as the slave surface.

6.5.6 Comparing results to manual calculations

Simulation results have been obtained for the two different axial settlement. In this subsection the hoop stresses of the segments are compared from the simulations to the manual calculations. Contour plots for hoop stresses at 1 mm and 26 mm can be seen in Fig. 23 and Fig. 25, respectively. Similar for both cases, is that the inner segment is in compression, indicated by the negative hoop stress, and the outer segment is in compression, indicated by the positive hoop stress. The absolute value of the maximum hoop stress in the outer segment is more than 1.5 times larger than in the inner segment. Throughout the slip joint length, the hoop stresses are nearly uniform. However, the stresses are increasing closer to the free end of the slip joint, especially in the outer segment.

Values of maximum stresses are larger in the simulations than in the manual calculations for compound cylinders. The compound cylinder problem was calculated with cross-sectional dimensions at the middle of the slip joint overlap. Therefore, a hoop stress value has been obtained by using the probe tool at one of the center nodes of the overlap. For the 26 mm axial settlement simulation this value was found to be $7.8e7$ Pa. Compared to the value from manual calculations for the outer segment of $6.5e7$ Pa, this is an 20% increase. Probed hoop stress values for one of the center nodes in the inner segment was found to be $-5.7e7$ Pa, which compared to the calculated value of $-4.8e7$ Pa is a 19% absolute value increase. The manual calculations may be indicative of the order of magnitude of stresses in the slip joint, however they do not accurately predict the stress magnitude.

Surface pressure contour plots has also been obtained for the two simulations of 1 and 26 mm, shown in Fig. 24 and Fig. 26, respectively. The simulations revealed that contact pressure at the inner surface of Segment 3, increased gradually from the top of the overlap towards the free end. Contact surface pressure at one of the center nodes of the slip joints was found to be $9.3e5$ Pa. Compared to calculated values of $7.7e5$ this is a 21% increase.

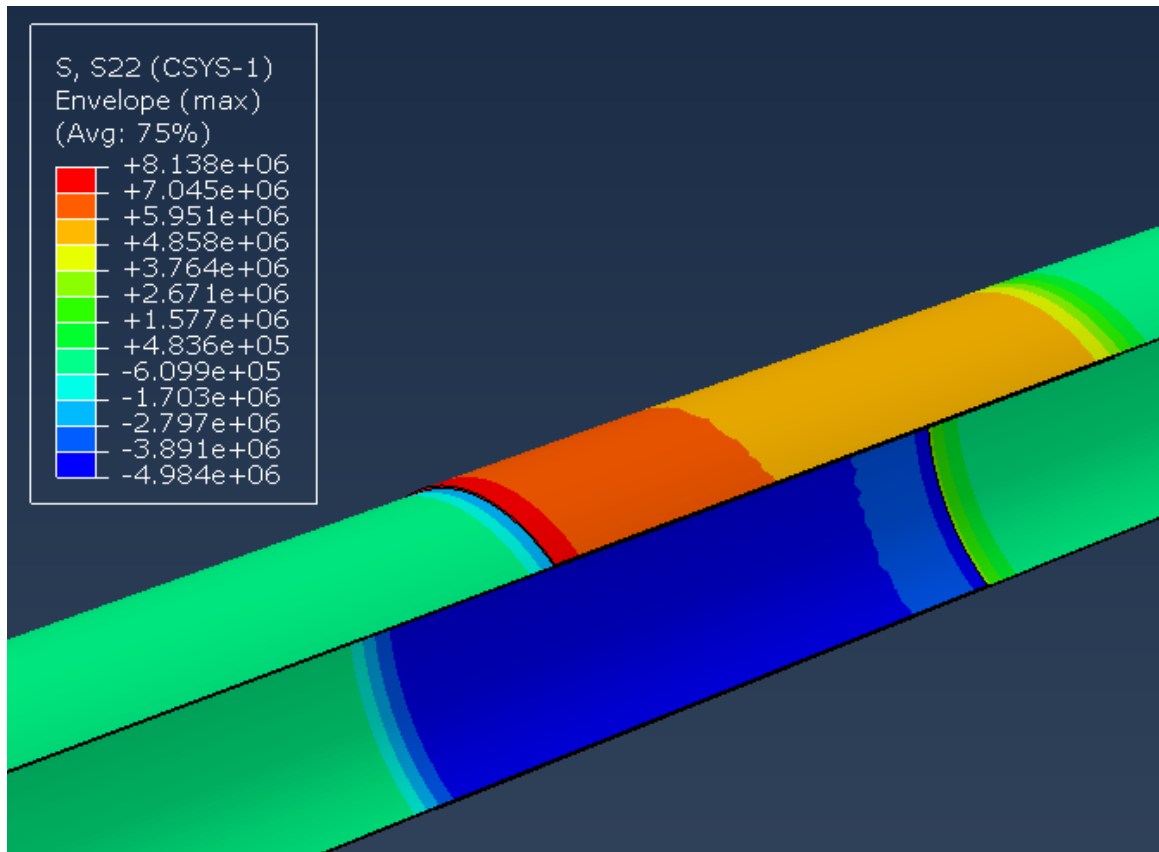


Fig. 23 – Contour plot of hoop stresses in Pa at approximately 1.16 mm axial settlement beyond initial contact.

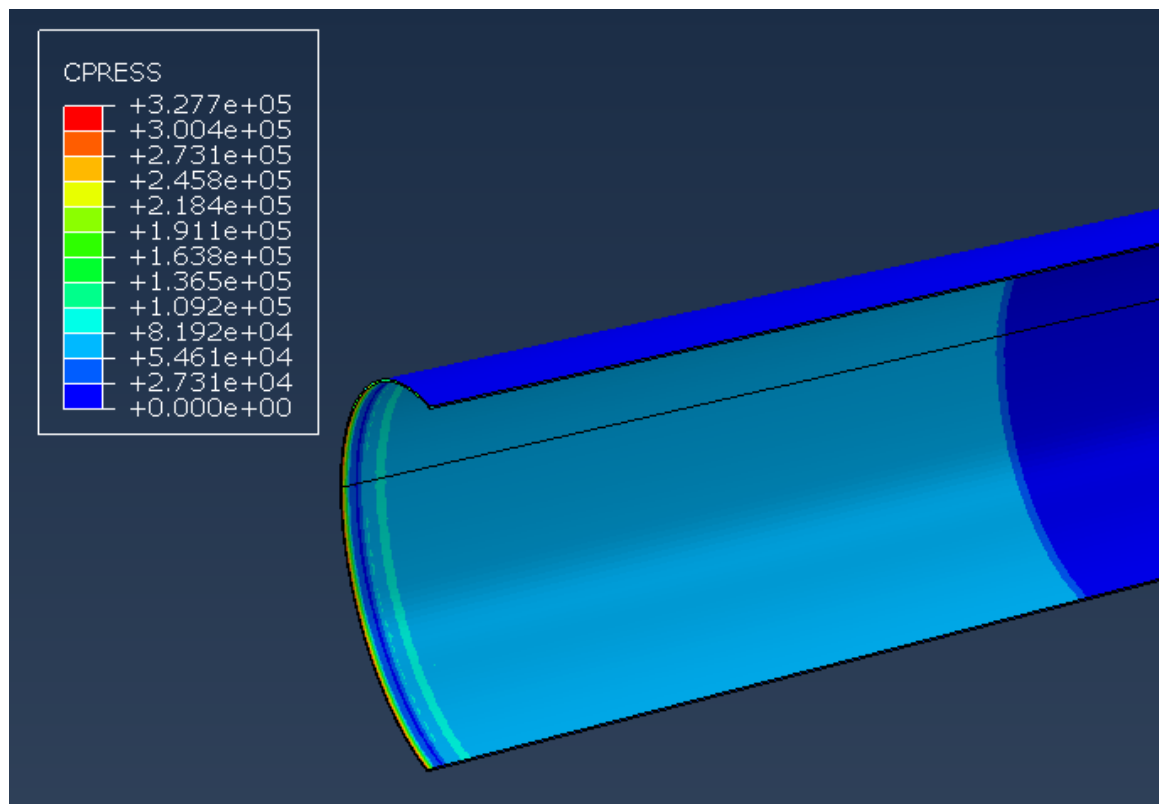


Fig. 24 – Surface pressure in Pa, for the inner surface of the top segment, with approximately 26 mm axial settlement beyond initial contact.

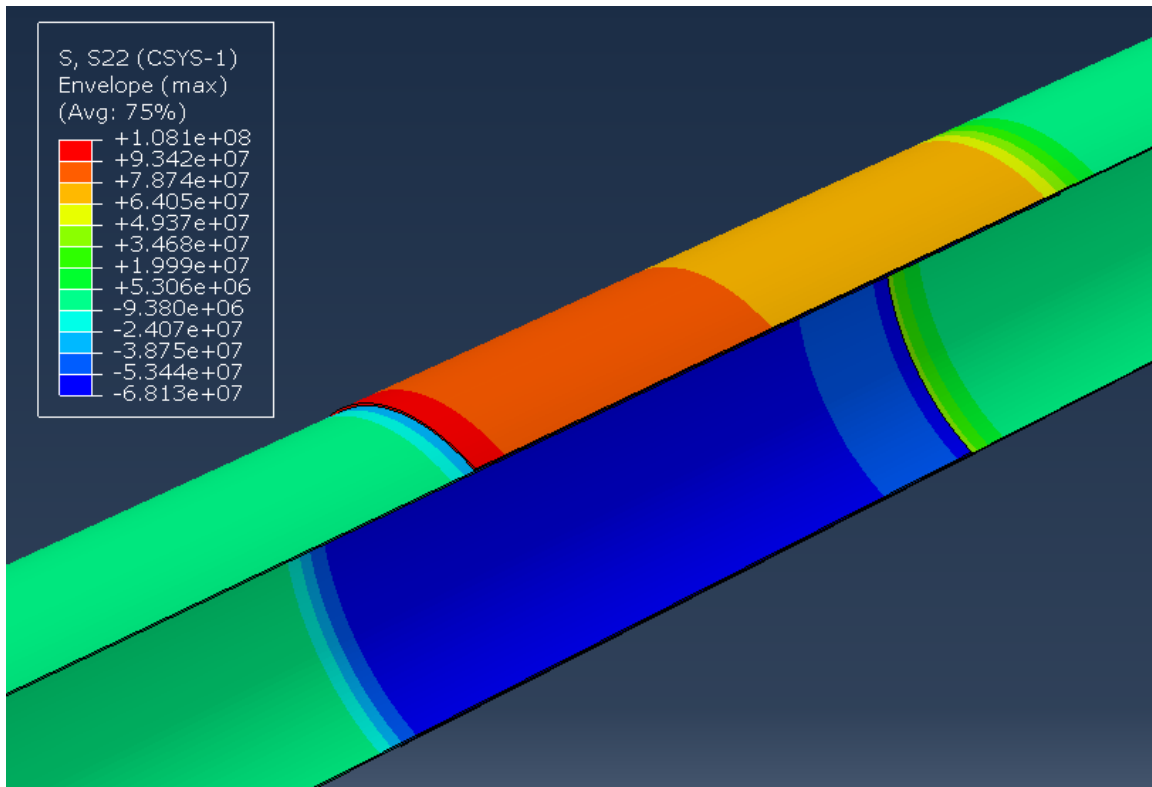


Fig. 25 – Contour plot of hoop stresses in Pa at approximately 26 mm axial settlement beyond initial contact.

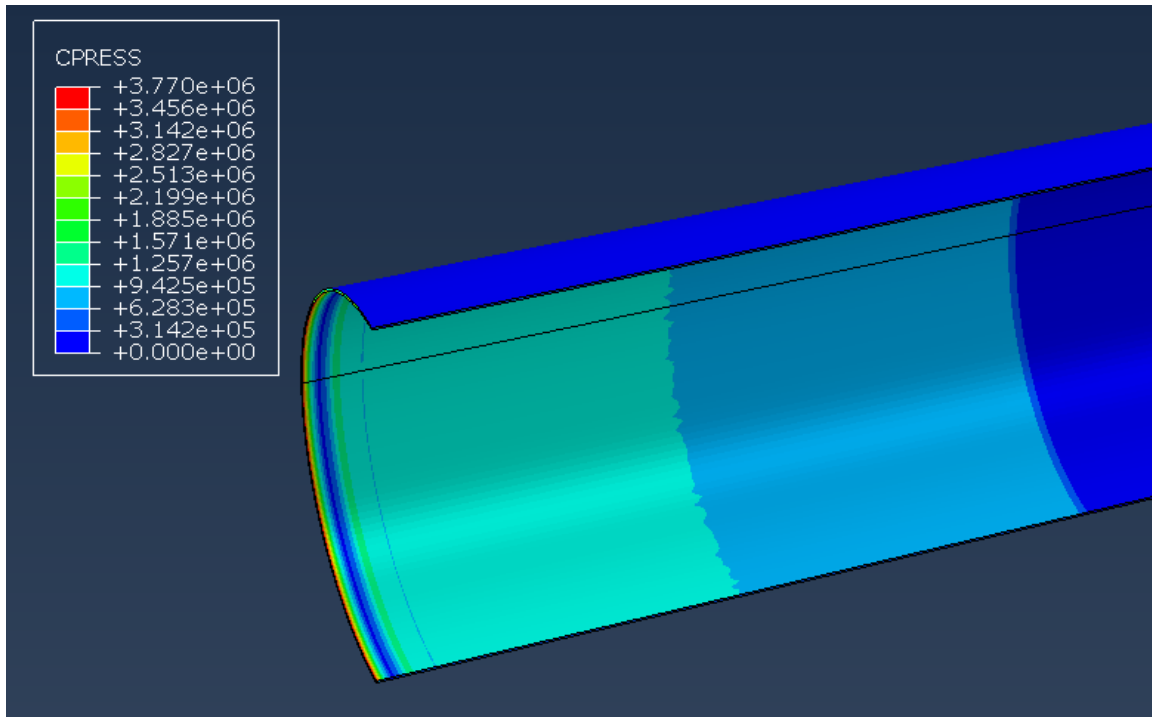


Fig. 26 – Surface pressure in Pa, for the inner surface of the top segment, with approximately 26 mm axial settlement beyond initial contact.

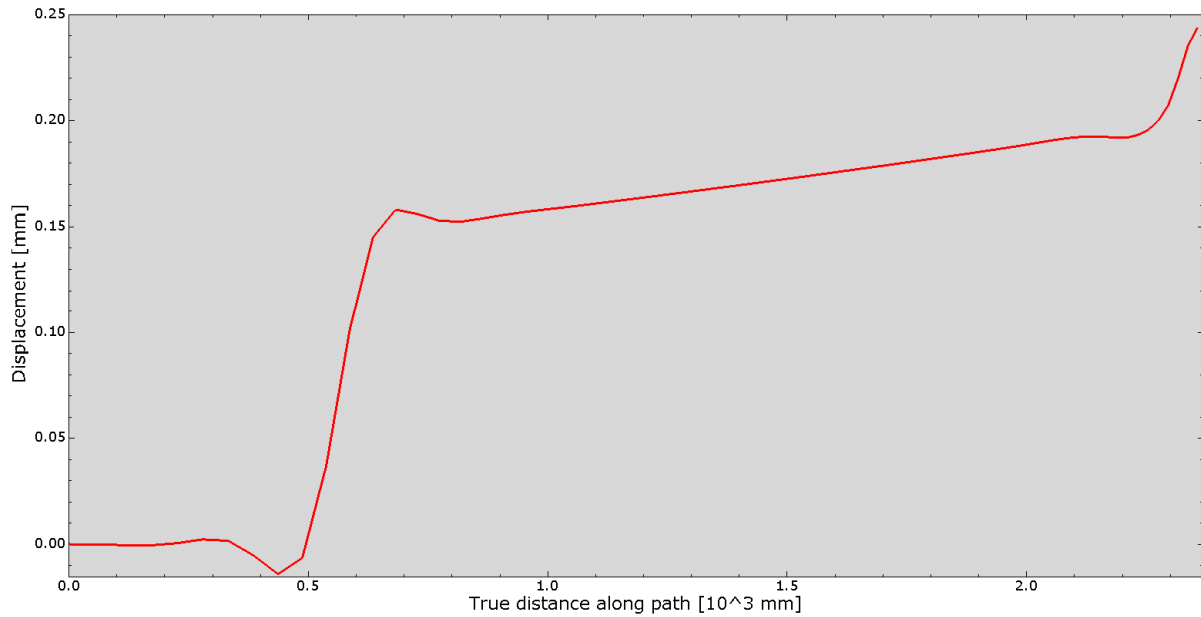


Fig. 27 – Radial deflection of the outer segment in the region of the slip joint, with axial settlement of 26 mm.



Fig. 28 – Radial deflection of a thin-walled cylindrical shell, calculated in Section 5.4.

The radial deflection of Segment 3 has been investigated so that it could be compared to the manual calculation for thin-walled cylindrical shells. A path was created in the axial direction along the slip joint at where values were obtained. The resulting radial deflection is plotted in Fig. 27, at 26 mm axial settlement. Fig. 28 shows the plot described in Section 5.4. Similarities between these two plots are visible in that both follow similar shapes. Not far away from the slip joint, the radial deflection of the segment is zero. Throughout the majority of the overlap, the radial deflection is constant at approximately 0.16 mm for the calculation. Radial deflection plotted for the finite element model is approximately constant but increases slightly towards the free end. Why this is the case, may be explained by the fact that the segments in the finite element model are tapered, whereas the manual calculation case is with constant diameter. Near the free end of the segment radial deflections increase more significantly.

6.6 Setup of the realistic model

6.6.1 General

The main model has been created with the intention of resembling the actual light pole geometry. However, dimensional variations within the tolerances are not considered and therefore the model is based on nominal dimensions found in the technical drawings. Nor has any potential imperfections introduced to the mast during manufacturing, storage or transport been included.

In the current section the geometry of the model is described, followed by an overview of the assigned element types and mesh. A contact formulation has been established which is assigned to regions in contact in the slip joint. Lastly, the steps, loads and boundary conditions created to simulate the full loading procedure is described.

6.6.2 Model geometry

Although the light poles contain three slip joints, only one have been included in the model in order to obtain results that are simple to interpret and to avoid simulations that are overly time consuming. The investigated slip joint is the middle one, as this is where the largest axial settlement was observed during the inspections. The nominal overlap length of this slip joint, between Segment 2 and Segment 3, is 1600 mm. Although Segment 2 and Segment 3 are 12,000 mm and 11,100 mm long, respectively, only 5000 mm of each of these have been modelled in order to decrease the total number of elements, and thus the computational time. It has been assumed that material far from the slip joint connection is not significantly influenced by deformations in the slip joint area, and therefore not modelled as part of the segments. The shortened sections of Segment 2 and 3 are modelled as two separate parts. Both segments have been modelled with a 16-sided polygonal cross-section, similar to the real light poles. According to pole dimensions in the technical drawings, tapers are differing slightly for the two segments, which results in contact initiating at one end of the slip joint before the other. As discussed in Section 4.2, The upper segment has slightly smaller taper than the bottom segment, meaning that contact initiates at the bottom of the slip joint.

To facilitate the pre-loading of the two segment pieces, handles comparable to those on the masts have been modelled. The exact dimensions for these are not given, but nor are they the point of interest in the analyses. A rough estimate is that these are 60 mm wide and 200 mm long. Two handles have been attached to either segment near the slip joint end, making the total number of handles to four. A tie constraint has been applied between the bottom of each handle to the surface where they are attached. The tie constraints connect two separate surfaces so that there is no relative motion between them (Dassault Systemes, 2019).

On either side of the shortened Segment 2 and Segment 3 beams have been attached, so that the full length of the masts has been included in the model. This is of importance when the model is upended and subsequently wind loads are applied to it. The beams are modelled by use of wire features which have been assigned circular beam profiles that have constant diameters throughout their lengths, meaning no taper is included. The beam wires are connected to the region containing the slip joint by multi-point constraints. This method constrains the motion of slave nodes, that being the end of a pole segment, to the motion of a single point which is the beam wire end. Thus, there is a seamless transition between the beam wire and the solid pole segment. The constraints used in the model are shown in Fig. 29, and the full model assembly with rendered beam profiles in Fig. 30.

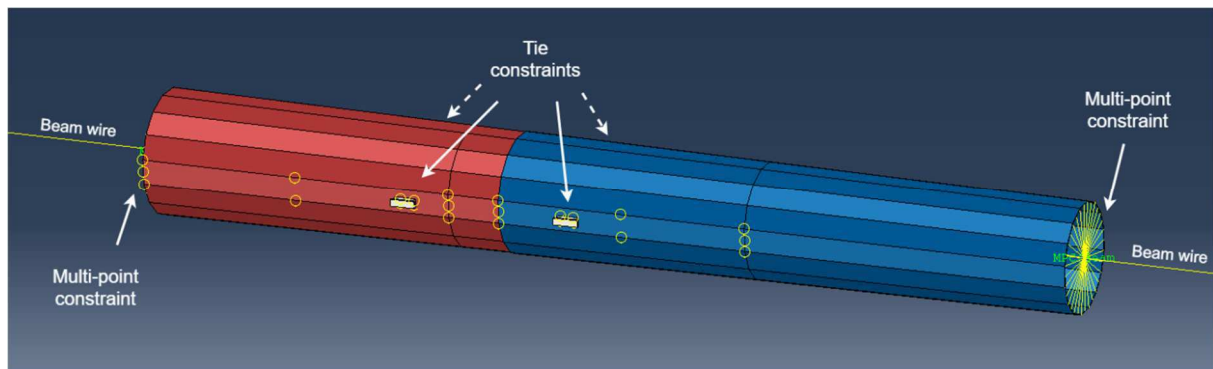


Fig. 29 – Indication of constraints used in the model. Multi-point constraints connect the beam wires to the end of solid pole segment, while four tie constraints attach handles to their respective mast segment surfaces.

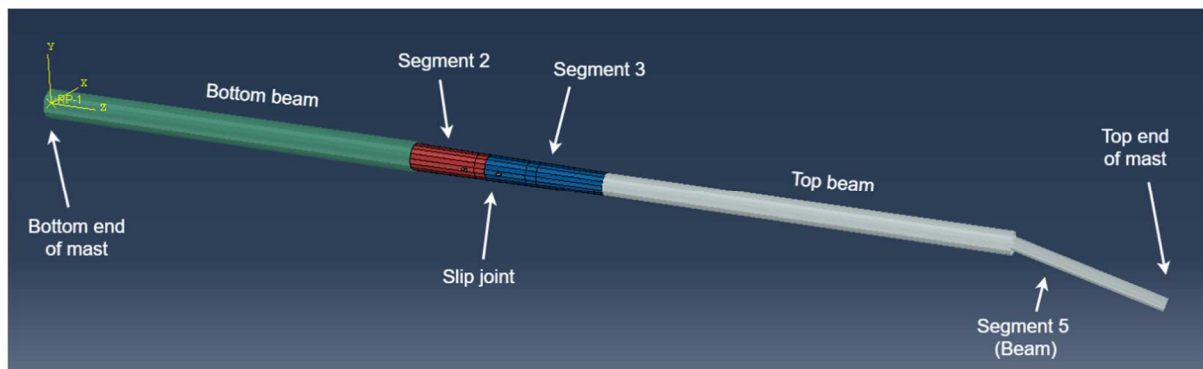


Fig. 30 – Full mast model. Segment 2, segment 3, and the slip joint between them indicated. Beam profiles have been rendered for better visibility.

Effort has been put into obtaining an identical mass of the model to the numbers given in the technical drawings. Due to the beam dimensions deviating slightly from the actual pole dimensions, evenly distributed non-structural mass has been assigned to these regions. Along the beam replicating Segment 5 several point masses have been added to resemble floodlights and the transverse beams at where they are attached. The point masses have rotary inertias, calculated from simplified geometries of floodlights and the large platform. As for the actual light poles, the total mass of the model is 12,400 kg.

6.6.3 Element types

There are three different types of features in the model: beams, solid pole segments and handles. Due to their different characteristics, unique element types have been assigned to each of the regions.

The pole regions containing the slip joint has been assigned continuum shell elements. Shell elements are selected due to the pole thicknesses being relatively thin compared to the other dimensions, such as length and diameter. The continuum shell elements are discretized based on a three-dimensional body, where the thickness of the shell is found from the part geometry. This has made it possible to model the three-dimensional geometry of the mast segments first, and followingly assign continuum shell elements (Dassault Systemes, 2019). The element type assigned is SC8R which is an 8-node hexahedron, general-purpose, finite membrane strains element with reduced integration. The 8-node continuum shell element is shown in Fig. 31.

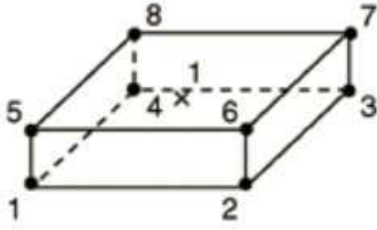


Fig. 31 – 8-node continuum shell element used for stress/displacement analysis, with node numbers and indication of integration point in the middle (Dassault Systemes, 2019).

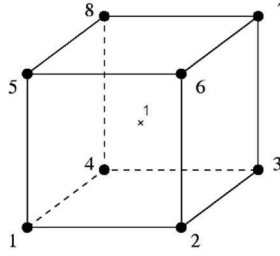


Fig. 32 – A 8-node solid continuum linear brick element with reduced integration (Dassault Systemes, 2019).



Fig. 33 – A 2-node linear beam element with node numbers and one integration point (Dassault Systemes, 2019).

The handles are solid parts and are therefore assigned a solid continuum element type called C3D8R. The C3D8R element is an 8-node linear brick with reduced integration and hourglass control. Reduced integration means that the element only has one integration point, located at the center. In a stress/displacement analysis this could result in hourglassing, i.e. uncontrolled distortion of the mesh, which is why the hourglass control has been enabled. The element is shown in Fig. 32. Lastly, the beam sections of the model have been assigned B31 elements, which is a 2-node linear beam in space. This element can be seen in Fig. 33.

6.6.4 Mesh

The regions of interest, which are the pole segments, are large components. Therefore, relatively many elements are made when the parts are meshed, especially if a fine mesh is applied. However, a very fine mesh results in a large number of elements which may increase the computational time unnecessarily. The pole segments have been meshed with only one element through the thickness. Each side of the hexadecagon profile has been seeded such that they are assigned six elements. In the longitudinal direction of the segments, seeds are assigned to the model so that resulting elements have aspect ratios close to 1 in the in-plane direction. The assigned element type is well suited for small thickness relative to the in-plane dimensions of the elements.

The beam sections are essentially just wire features and have therefore only been meshed in one direction. Relatively few elements were required to mesh these, compared to the slip joint region. Handles are small components and have been meshed relatively fine without increasing the total element number significantly.

6.6.5 Contacts

The contact that has been defined in the current model is a surface-to-surface contact pair. For this type of contact definition two surfaces that potentially could be in contact during the simulations have been selected. The only regions where contact properties had to be defined in the model was on the surfaces of the slip joint potentially in contact. The outer surfaces of Segment 2 were set as the master surfaces, while the inner surfaces of Segment 3 were set as the slave surfaces. A master-slave assignment means that the master surface can in principle penetrate the slave surface, but not the other way around (Dassault Systemes, 2019).

The property of the contact is defined both in terms of a normal and a tangential behavior. The normal contact behavior is defined by a pressure-overclosure relationship called “Hard” contact. This relationship means that there is zero contact pressure when the surfaces are

separated, and when in contact, any surface pressure can appear. The setting that allows for separation after contact, was enabled. The tangential behavior was defined by a penalty friction formulation, and the coefficient of friction set to $\mu=0.6$. Defined contact surfaces with the mentioned contact properties can be seen in Fig. 34.

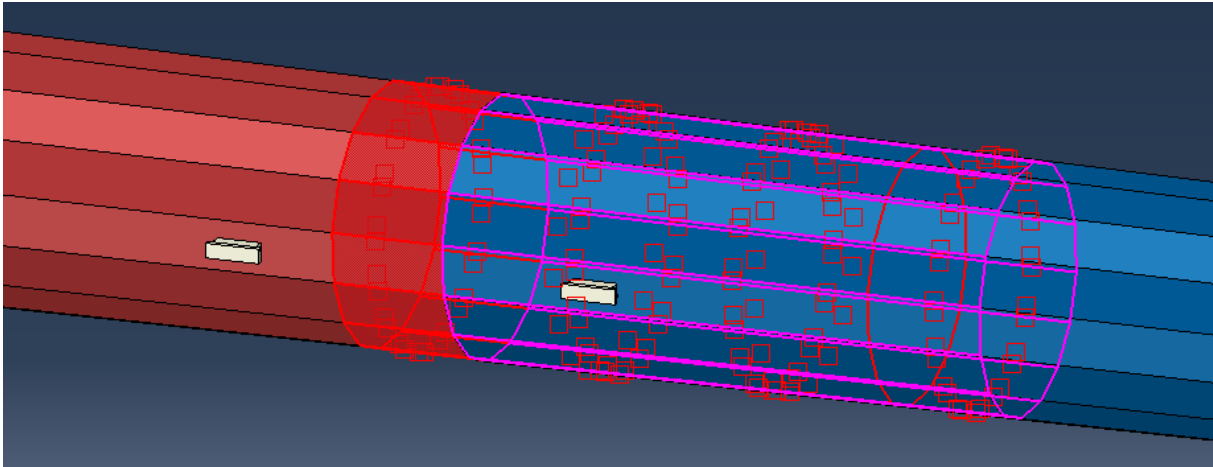


Fig. 34 – Contact surfaces defined for the model in the slip joint region. The red surface (master) is assigned to outer surfaces of segment 2. The pink surface (slave) is assigned to the inner surfaces of segment 3.

6.6.6 Steps

The current subsection describes the sequence of steps that has been created to simulate the full procedure from assembling of the light pole to several years of operation. Although the loading procedure discussed in Subsection 6.3.3 only consists of three stages, the whole simulation has been divided further into more steps. A total of six analysis steps has been created, all listed in Table 4. The first analysis step is the introduction of a controlled displacement which ensures that initial contact in the slip joint connection is obtained. Followingly, the pre-loading of the slip joint was performed in the second analysis step, where the two segments are pressed together. Ahead of the upending procedure, gravitational forces are introduced to the model in step three. Upending of the mast from laying horizontally to standing vertically is performed in analysis step four. Followed by the upending step a step has been included where the model is allowed to find its static upended position. The sixth analysis step is where wind loads are applied to the model.

All the steps have been carried out through either a static or quasi-static analysis. The static steps do not have a natural time scale in this case, i.e. the length of the step does not affect the solution. Therefore, all static steps have been given a step time of 1 and the initial increment size has been set to 0.01. The quasi-static steps have been given more realistic time scales, e.g. the upending step was given a total step time of 90 s. To this step, a maximum increment size of 1 has been applied, thus the light pole is never rotated more than 1° from each increment to the next, as the rotation increment cannot be too large. Similarly, the wind load step which has been given a total step time of 1000 s, has a maximum increment size of 10 s. Output has been requested at every 10 s of time such that all the peaks and valleys of the amplitude curve are included in the calculation. A quasi-static analysis is useful when inertia effects can be neglected and the static response at the end of the simulation is most important (Dassault Systemes, 2019).

The “NLgeom” setting has been toggled on for all the analysis steps, meaning that Abaqus accounts for geometric nonlinearities in the model. Geometric nonlinearity must be accounted for when large deflections or rotations are present (Dassault Systemes, 2019), which is the case during the current simulation procedure.

Table 4 – Tabulated sequence of analysis steps for the finite element model, including type of analysis and step time.

Step number	Name	Type (Application)	Step time
1	Displacement control	Dynamic (Quasi-static)	1
2	Pre-loading	Dynamic (Quasi-static)	10
3	Applying gravity	Static	1
4	Upending	Dynamic (Quasi-static)	90
5	Static settlement	Static	1
6	Wind loads	Dynamic (Quasi-static)	1000

6.6.7 Loads and boundary conditions

The loads and boundary conditions are changing from step to step throughout the simulation. However, there is some consistency in that boundary conditions remains the same in some of the steps.

6.6.7.1 *Displacement control and pre-loading*

During the first two steps, i.e. while the controlled displacement and the pre-loading pressure is applied, the light pole is fixed in all degrees of freedoms at the bottom end of the model. The top end of the model is constrained in all degrees of freedom except DOF 3, meaning movement in the axial direction of the mast is allowed.

Prior to the simulations, the two pole segments have been assembled with an overlap of 1745 mm between them while there is still a small radial gap, meaning there is no contact occurring between segments in the slip joint region. To initiate the first contact in the slip joint, the controlled axial displacement has been applied at one end of the mast model. The other end of the model, that being the very bottom of the mast, has been fixed in all the degrees of freedom. Thus, the displacement, which was set to just 4 mm, presses the two segments together and contact appears in the slip joint.

After the initial contact has been obtained through the controlled displacement, the pre-loads are applied in terms of surface pressures on the assembling handles. The application of pre-loading to the handles is shown in Fig. 35, indicated by the pink arrows. The part of the model colored red is the fixed segment, while the part colored blue is the segment that is allowed to slide axially.

A pressure of 1.67×10^7 Pa has been applied to all handles, causing a total compressive force of 100 kN set to tighten the slip joint further. During the pre-loading step, the pressure is gradually increased as defined by the amplitude curve shown in Fig. 36. The full pre-load pressure is reached after 8 s and remains applied for the last 2 s of the step to ensure that a final static state of the pre-loaded slip joint is reached.

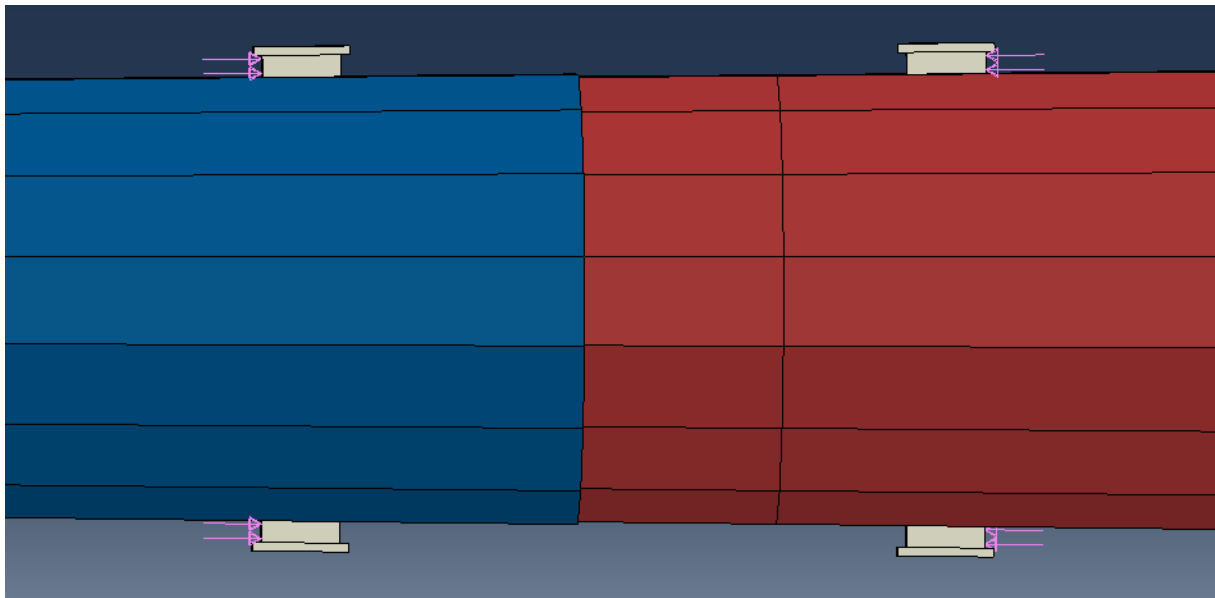


Fig. 35 – Pre-load pressures, indicated by pink arrows, applied to handle surfaces. The pressure applied to either handles on either segment are oppositely directed, to resemble an assembling procedure with the use of hydraulic jacks.

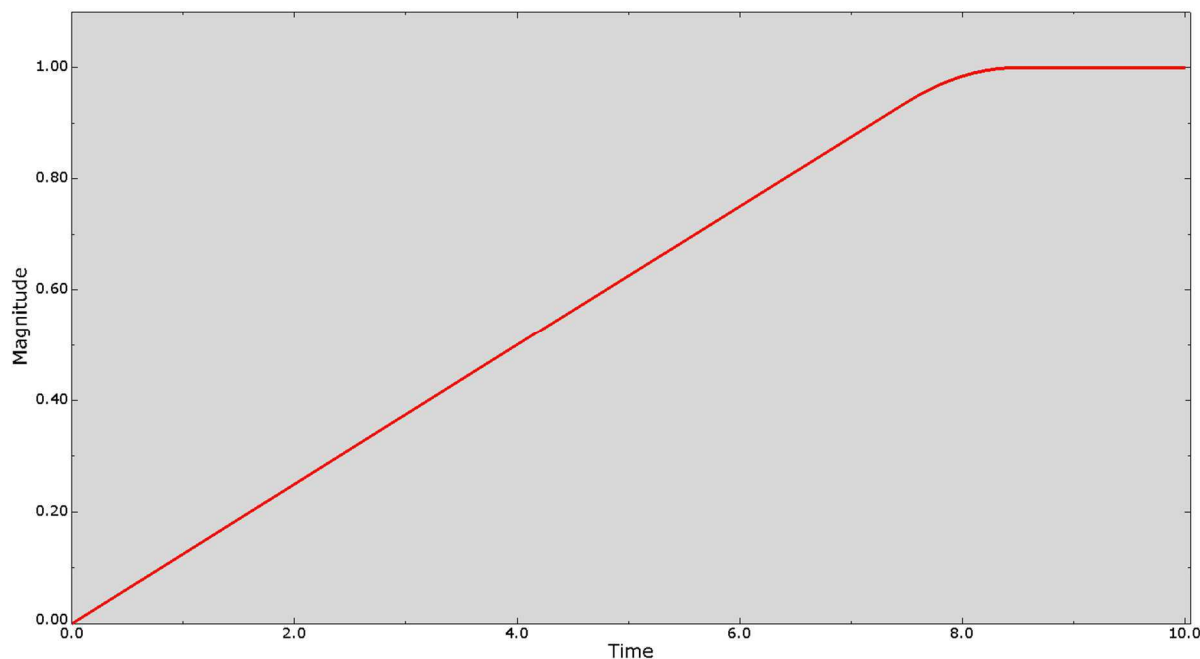


Fig. 36 – Amplitude curve for the pre-load pressure. The pre-load pressure is ramped up from 0 to 1 times its maximum value during the first 8 s of the step. The pressure is held at its maximum value for 2 s to ensure that a final static state of the assembled slip joint is obtained.

6.6.7.2 Applying gravity, upending and allowing static settlement

After the slip joint connection has been pre-loaded, the gravitational force is applied to the model. The gravitational force has deliberately been excluded from the two previous steps to simplify the pre-loading procedure but becomes of importance during the upending and wind load steps. The gravity load is defined to act in the negative y-direction with a magnitude of 9.81 m/s^2 . In this step both ends of the model are constrained in all degrees of freedom except UR1, i.e. rotation about the x-axis. The reason for not constraining this degree of freedom is that it is the same axis which the model rotates about during the following upending step.

During the upending procedure, the whole model is rotated 90° about the x-axis, so that the mast eventually is standing vertically at the end of the step. This has been done by keeping the bottom boundary condition from the previous step, i.e. rotation around the x-axis is free while all other degrees of freedom are constrained. The upending motion is facilitated by applying a rotational displacement at a reference point placed in the same location as the bottom of the model. This reference point has only been tied to the very top node of the model and only in the 4th degree of freedom (UR1). Rotational displacement applied in the reference point thus rotates the top node of the model with the reference point acting as a rotation centre. At the beginning of the step, the constraint at the top of the model from the previous step has been removed.

After being upended, a boundary condition has been applied at the bottom of the mast, constraining all degrees of freedom at its current position. Thus, the mast is fixed at the bottom while standing vertically. No other boundary conditions are active in the model at this state.

6.6.7.3 Wind loads

The boundary conditions remain the same as from the previous step while wind loads are applied to the model, meaning that the light pole is only fixed at its bottom. This is meant to

resemble the mast being bolted to the foundation. The loads which are applied along the beam elements of the model has previously been described in Subsection 6.3.3.

6.7 About the parameter studies

Parameter studies has been performed to investigate how the changes in different parameters of the model influences the behavior of the slip joint connection. Primarily, the extent of axial settlement was the point of interest for each individual study.

The parameter studies have been performed by running several simulations where only the value of one parameter was changed at a time. First a parameter study concerning the variations of pre-load forces was carried out, followed by a study of variations in the coefficient of friction.

6.7.1 Study 1: Variations of pre-loading

The reason for studying different pre-load forces is that the magnitude of applied pre-load forces is modifiable and can be defined prior to assembling. A hypothesis is that less axial settlement will occur during operation with increasing pre-load forces, due to the slip joint being assembled tighter.

Simulations have been carried out with five different pre-load forces: 80 kN, 100 kN, 120 kN, 200 kN and 300 kN. The pre-loading of 100 kN is just above the axial compressive force on the slip joint due to the mass of the structure, multiplied by a factor of 2. Simulations with pre-load forces of 80 kN and 120 kN have been performed to investigate the resulting axial settlement of $\pm 20\%$ pre-load. These are relatively small changes in the pre-load force. The simulation with pre-load force of 200 kN and 300 kN has been performed to investigate the results of a more severe pre-loading.

6.7.2 Study 2: Variations of coefficients of friction

The effect of various coefficients of friction on the slip joint connection has been studied due to the uncertainties related to it. Unlike the pre-load forces, the coefficient of friction is not a parameter that is simple to adjust for the actual light poles. Furthermore, the coefficient of friction that has been defined in the contact formulation for the model is for static friction. For kinetic friction, i.e. when sliding occurs, the coefficient of friction is in general significantly smaller. Therefore, only values smaller than the one used in the base calculation has been included in this parameter study. The three investigated values of coefficient of friction are 0.6, 0.5 and 0.4.

7 Results from Finite Element Analyses

This chapter presents the results from key instants during pre-loading and upending, followed by the results of a static wind analysis and the resulting axial settlement from the series of five large storms. Findings from the two parameter studies are also shown and described.

7.1 Maximum stresses during assembling and upending

Stresses in the structure have been checked for stages before wind loads are applied. The two instants of highest interest are when the slip joint has been pre-loaded and during upending, whether any large stresses appear in the structure.

7.1.1 Results of pre-loading

A contour plot for hoop stress in the slip joint region at the beginning of the assembling process is shown in Fig. 37. A clear pattern emerged, in that stress concentrations appeared at corners of the pole. The outer segment is in tension, whereas the inner segment is in compression indicated by the negative hoop stress values.

A similar contour plot for hoop stress has been obtained when the slip joint has been fully pre-loaded with 100 kN, shown in Fig. 38. The visible pattern of stress at corners around the pole has diminished. Stresses at the nearest corners to handles where pre-load has been applied, are larger than other corners around the pole. In these two corners, the hoop stress is 30 MPa at full pre-load. However, the largest stress concentrations in the model with all pre-applied appears around handles.

A contour plot of the surface pressure at the inner surfaces of Segment 3, shown in Fig. 39, reveal that there is not full contact in the slip joint. Contact has merely occurred at corners of the pole geometry.

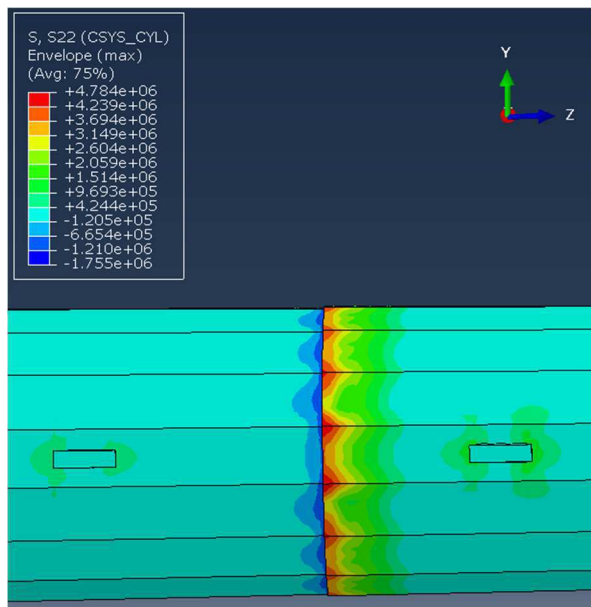


Fig. 37 – Hoop stress in slip joint region during assembling, with approximately 1% of pre-load applied. Segment 2 (left) is in compression and Segment 3 (right) is in tension.

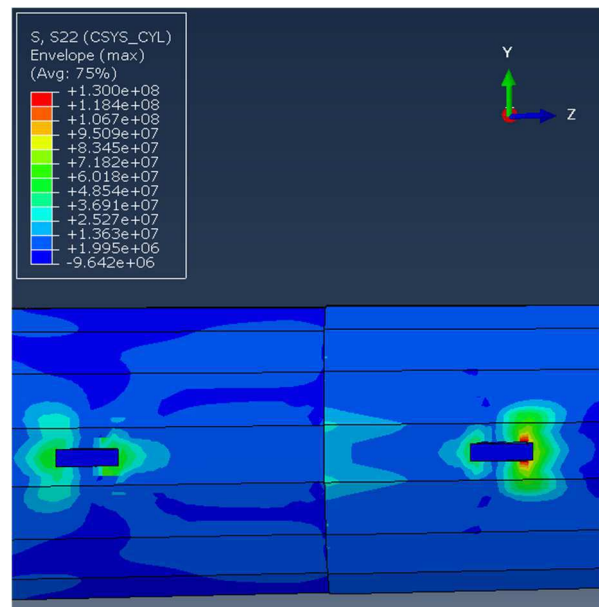


Fig. 38 – Hoop stress in slip joint region with 100% of pre-load applied. Stress concentrations emerges around handles.

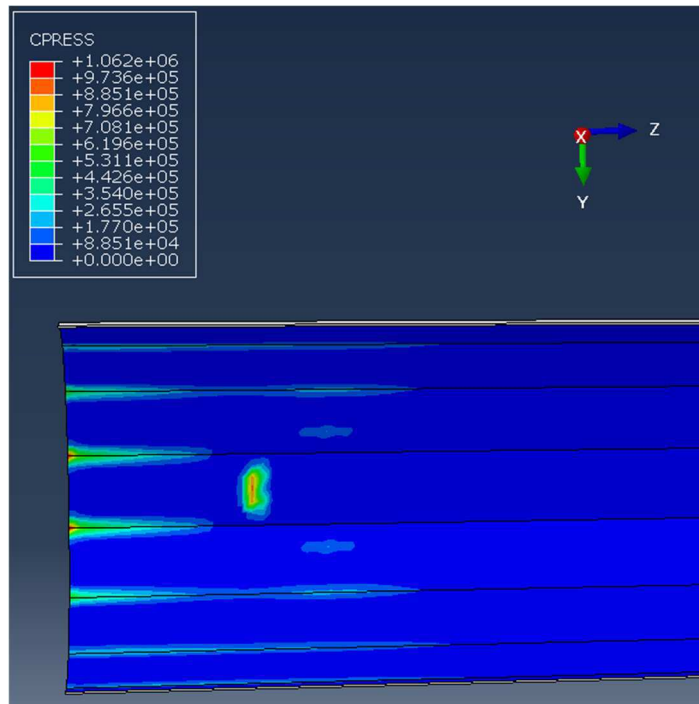


Fig. 39 – Surface pressure in Segment 3 after pre-loading.

7.1.2 Stresses during upending

The largest stresses in the model during the upending procedure appeared about halfway through, when the structure was at 42° tilt from the ground. Maximum von Mises stress is found to be 246 MPa, a few meters above the slip joint connection, as shown in Fig. 40. This is on the side facing upwards, meaning that it is compressive stress.

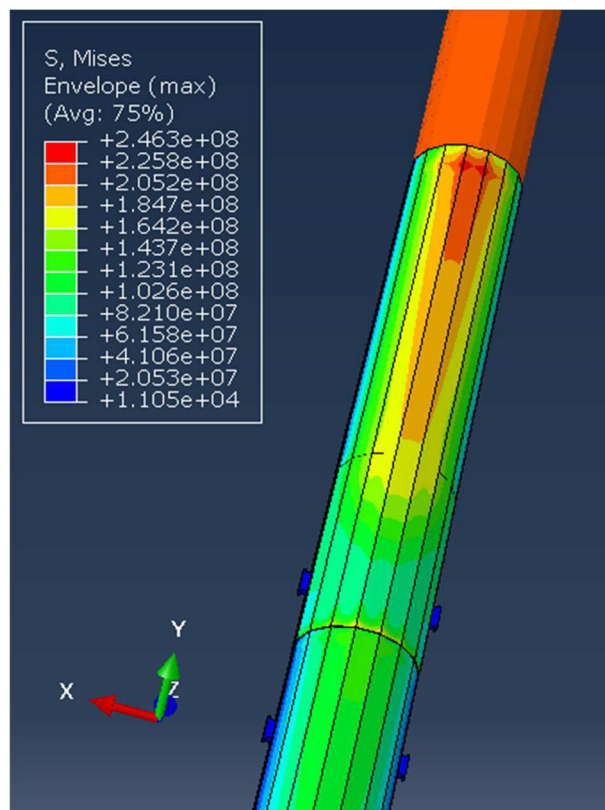


Fig. 40 – Maximum von Mises stress of 246 MPa in light pole during upending.

7.2 Result of static wind loads

Static wind loads with a loading factor of 1 have been applied to the model at its upended position. To ensure that the wind loads applied to the model were relatively similar to calculated values, the reaction moment was investigated at the bottom of the mast. This value was found to be 1.75e6 Nm which compared to the calculated value is just an increase of 2.6%. Reaction moment due to the weight of floodlights was not included in the previous wind calculation, which would bring the two numbers even closer.

The largest von Mises stresses in the structure with static wind loads applied was found to be 182 MPa, i.e. well within the elastic region of the material. A region of the plotted von Mises stress contours on the deformed light pole is shown in Fig. 41. The greatest stress concentrations appeared in corners at the bottom of the slip joint connection, in the direction which the wind acts. With a loading factor of 1.5 the contour plot exhibit similar stress patterns, shown in Fig. 42. The maximum von Mises stress in the model has been found to be 266 MPa, still below the yield point.

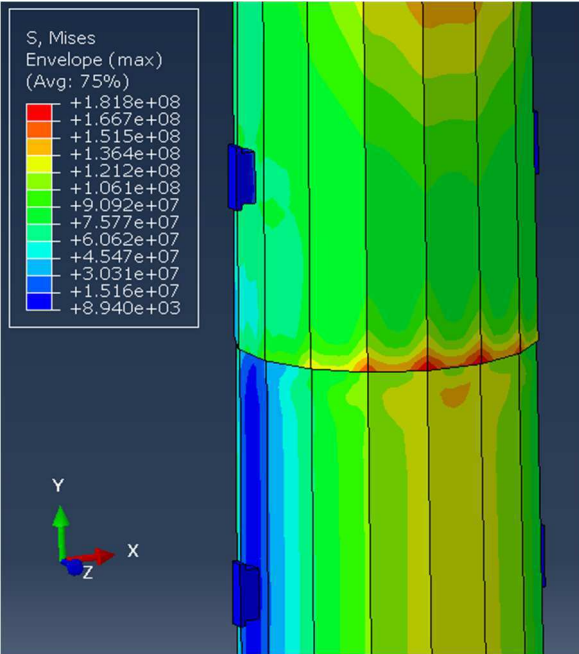


Fig. 41 – Contour plot showing von Mises stress concentrations at corner nodes at bottom of the slip joint connection. Wind scaling factor of 1 resulting in a maximum stress of 182 MPa.

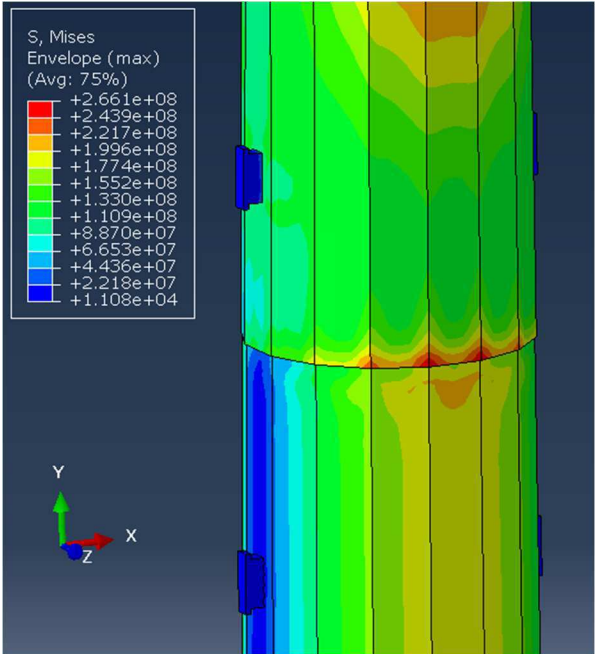


Fig. 42 – Contour plot showing von Mises stress concentrations at corner nodes at bottom of the slip joint connection. Wind scaling factor of 1.5 resulting in a maximum stress of 266 MPa.

7.3 Axial settlement with quasi-static wind loads

Values for axial displacement in the slip joint has been obtained at several stages throughout the simulation, shown in Fig. 43. The axial displacement is measured in terms of change in overlap length from initial contact, which is found by measuring the distance between two nodes laying along an edge in contact, one at the top of Segment 2 and one at the bottom of Segment 3. This distance has been found at nine instants during the simulation: after each of the steps simulating initial contact, pre-loading, upending, letting the light pole stand freely and after each of the five storms.

Pre-loading with 100 kN resulted in an axial displacement of almost 2 mm from initial contact. Some further displacement was experienced during the upending procedure. After the mast has been upended and is allowed to stand freely, it experiences no significant axial settlement.

All the five storms contribute almost equally to the total axial displacement found to be 3.22 mm. Measured as an axial settlement after pre-load has been applied, this value reduces to 1.3 mm. The axial settlement does however not show any signs of stagnation from storm to storm; in fact, the last storm causes the second largest contribution to axial settlement of all the storms.

To investigate whether the axial settlement decreases over time, the same series of five storms has been applied to the model once more. This resulted in 0.77 mm axial settlement during the last five storms compared to 1 mm during the first five, meaning a 23% decrease which imply that the axial settlement in the slip joint is in fact slowing down.

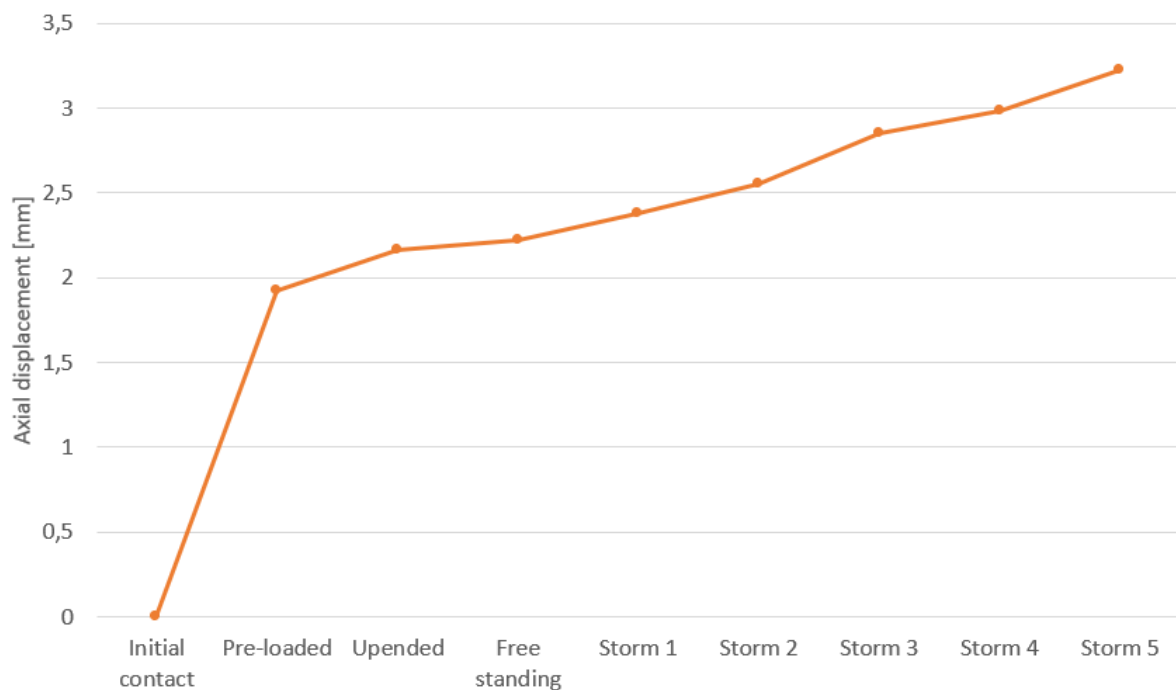


Fig. 43 – Axial displacement in slip joint after initial contact between segments has occurred.

7.4 Parameter study 1: Pre-load force

The first investigated parameter of the slip joint was the pre-load force used to tighten the slip joint connection. Five simulations with different magnitudes of applied pre-load has been carried out. Two different plots have been created; one showing axial displacement past initial contact and one showing axial settlement after the slip joint connection has been pre-loaded.

In Fig. 44, all the curves of axial displacement yield relatively similar shapes. Larger pre-load force expectedly resulted in larger axial displacement during assembling. Comparing the axial settlement with 100 kN pre-load to simulations with 80 kN and 120 kN resulted in 83% and 116% of the axial settlement respectively. For the two cases where even larger pre-loads were used, i.e. 200 kN and 300 kN, 176 % and 233% axial displacement experienced in the 100 kN case, were obtained. Therefore, the application of pre-loads to axial settlement do not hold a linear relationship.

Fig. 45 has been plotted to better visualize the slip joint behavior after it has been pre-loaded. The plot shows that smaller pre-loads subsequently results in larger axial settlement. Simulations with lower pre-loads are shown with a steeper curve, implying that axial settlement has not stagnated for those cases. An interesting observation of the plotted curve in Fig. 45, is that the total axial settlement reduces slightly during the fourth storm for high pre-load forces.

It can be concluded that less axial settlement occurs after a larger pre-load has been applied. The 300 kN curve in Fig. 44 do not increase significantly after being pre-loaded, where the amount of axial settlement was 0.39 mm. Compared to results with pre-loading of 100 kN this was an axial settlement of just 30%.

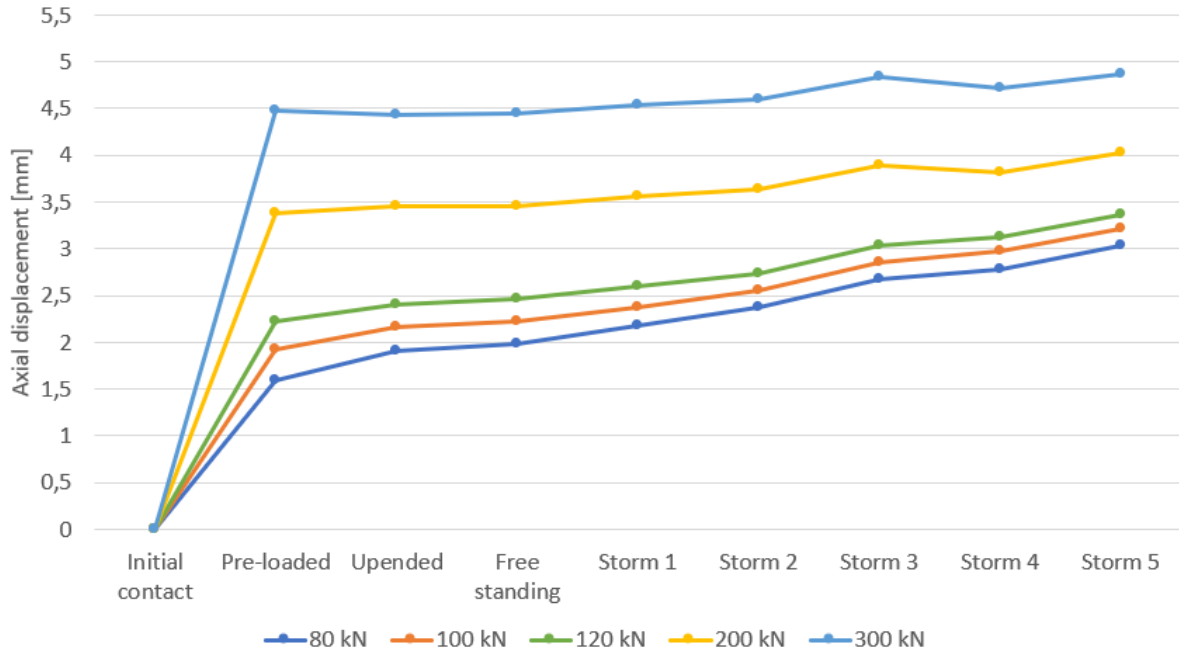


Fig. 44 – Axial displacement in slip joint, for five different pre-loads, measured from initial contact between segments.

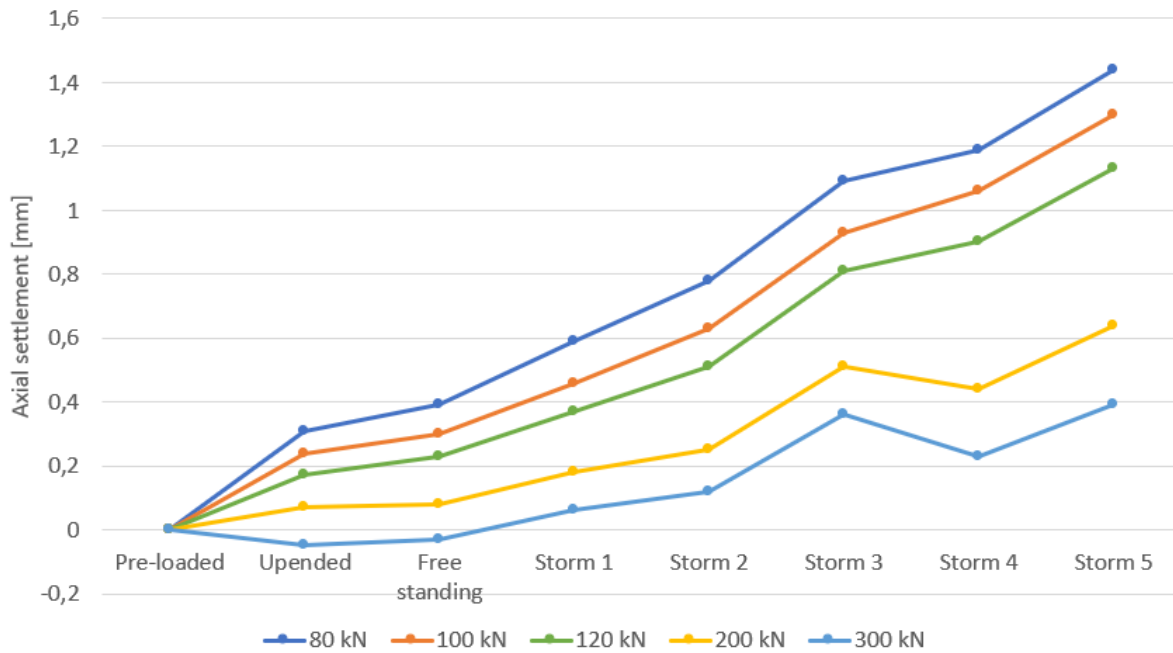


Fig. 45 – Axial settlement in slip joint, for five different pre-loads, measured after the connection has been pre-loaded.

7.5 Parameter study 2: Coefficient of friction

The second investigated parameter of the slip joint was the coefficient of friction. Three simulations with different COFs defined in the contact formulation has been carried out. As for the study of pre-load, two different plots have been created; one showing axial displacement past initial contact and one showing axial settlement after the slip joint connection has been pre-loaded.

The three curves in Fig. 46 shows that changes in the coefficient of friction did also yield relatively similar shapes. Axial displacement experienced during the pre-loading was larger for smaller values of coefficient of friction.

The plot in Fig. 47 show that the amount of axial settlement experienced after pre-loading is relatively similar for all three coefficients of friction. Slightly more axial settlement has been obtained with smaller coefficients of friction. Compared to the simulation with μ of 0.6, the increased axial settlement with μ equal to 0.4 and 0.5 was just 13% and 2% respectively.

The results may indicate that more axial settlement in general occurs with smaller coefficient of friction. The fact that axial settlement increases in the last storm imply that the axial settlement is yet to stagnate, and therefore it is difficult to predict whether more axial settlement of significance has occurred with a smaller COF upon stagnation.

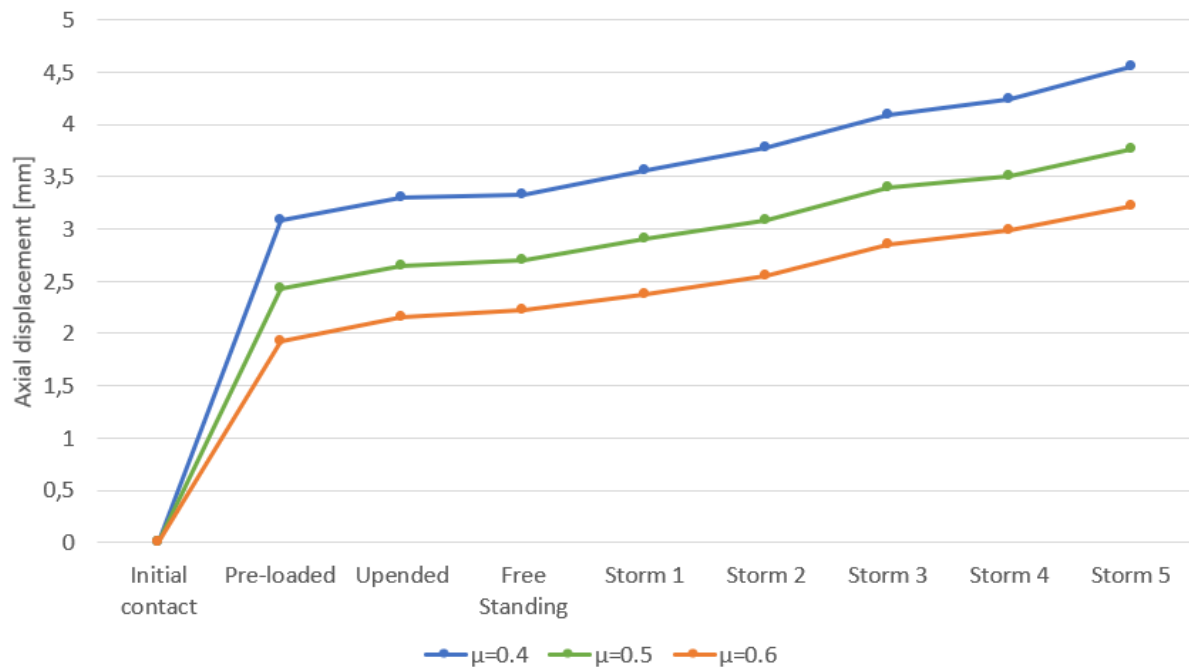


Fig. 46 – Axial displacement in slip joint, for three different coefficients of friction, measured from initial contact between segments.

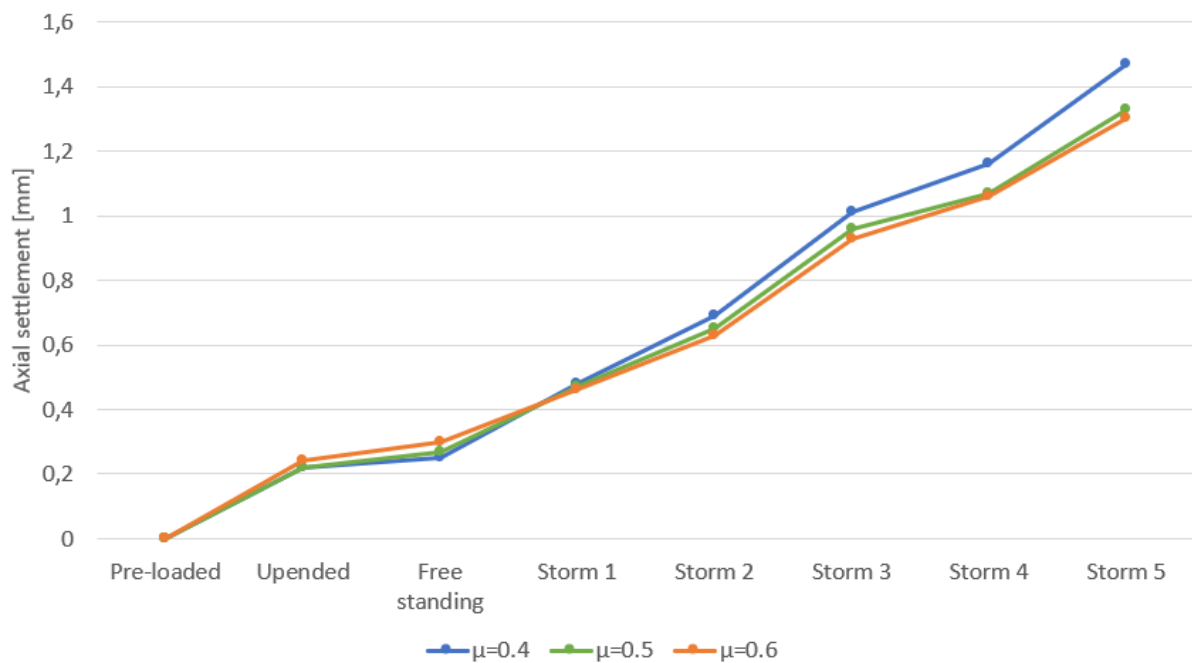


Fig. 47 – Axial settlement in slip joint, for three different coefficients of friction, measured after the connection has been pre-loaded.

8 Conclusions and Further Work

8.1 Conclusions

The thesis aimed to study the settlement phenomena of light poles with slip joint connections by using finite element analyses. This has been done through a simulation procedure consisting of six steps, including the pre-loading, upending and application of wind loads.

The simulation where 100 kN pre-load force was applied to the slip joint connection, resulted in an axial settlement of 1.3 mm. This value is not nearly as severe as for one of the real masts where an axial settlement of 26 mm had been observed during inspection. A likely explanation for the lack of axial settlement is the simplified wind model. It has been designed to represent a series of large storms acting from different directions, all including eight periods of slow oscillations just below their peak value. Compared to the full operational time of the light poles, these storms do only represent a fraction of the actual time span. More axial settlement can be expected for a longer wind history, as the amount of axial settlement did not seem to stagnate during the series of storms.

The first parameter study, where different magnitudes of pre-load force was simulated, revealed that increasing the applied force caused larger axial settlement during pre-loading but less axial settlement throughout the remainder of the simulation.

The second parameter study, where the coefficient of friction was varied, showed that lower coefficient of friction resulted in more axial displacement during the entire simulation. The amount of axial settlement was larger during each of the storms with the lowest coefficient of friction, implying that a lower coefficient of friction causes more rapid axial settlement in the slip joint connection.

8.2 Further work

The extent of axial settlement obtained through the simulations was relatively small compared to observation for the actual light poles. Using a wind history that represents a longer time span will likely yield larger axial settlements for the slip joint, and therefore this of interest. With sufficiently long wind simulations, one could also investigate whether the axial settlement stagnates and reaches a limit, meaning the slip joint reaches an equilibrium.

Another aspect that has likely had an influence on results is that simulations has been performed with quasi-static application. Including dynamic effects of the wind may yield a larger amount of axial settlement. The effect of gusts and the many high-frequency oscillations of the wind can be studied.

An investigation of how variations within fabrication tolerances influence the slip joint connection is of curiosity. As previously described, differences in cone angles determines where initial contact occurs, and therefore this is a topic of interest.

References

- BARONE, B. 2014. *Back to Basics: Slip Fit Pole Assembly Procedure* [Online]. Available: <https://web.distran.com/blog/bid/108952/back-to-basics-slip-fit-pole-assembly-procedure> [Accessed 30.01.20].
- CALLISTER JR., W. D. & RETHWISCH, D. G. 2014. *Materials Science and Engineering, Ninth Edition*, Asia, Wiley.
- DASSAULT SYSTEMES 2019. SIMULIA User Assistance 2019.
- DICLELI, M. & NASSAR, W. 2003. Practical approach to optimum design of steel tubular slip-joint power transmission poles. *WIT Transactions on The Built Environment*, 67.
- DNV GL 2014. Design of Offshore Wind Turbine Structures.
- DNV GL 2015. Tilstandsvurdering av lysmaster (name hidden) stadion.
- DNV GL 2019. DNVGL-RP-C208 Determination of structural capacity by non-linear finite element analysis methods.
- ENCYCLOPÆDIA BRITANNICA. 2020. *High-rise buildings* [Online]. Available: <https://www.britannica.com/technology/construction/High-rise-buildings> [Accessed 23.06.20].
- EUROCODE APPLIED. 2009. *Table of design material properties for structural steel* [Online]. Available: <https://eurocodeapplied.com/design/en1993/steel-design-properties> [Accessed 09.06.20].
- FENNER, R. T. 1986. *Engineering Elasticity*, Great Britain, Ellis Horwood Limited.
- NORSK ELEKTRONISK KOMITE 2012. NEK EN 50341-1:2012 Overhead electrical lines exceeding AC 1 kV.
- NORWEGIAN METEOROLOGICAL INSTITUTE. 2020. *eKlima - Free access to weather- and climate data* [Online]. Available: http://sharki.oslo.dnmi.no/portal/page?_pageid=73,39035,73_39049&_dad=portal&_schema=PORTAL [Accessed 10.03.20].
- BERG, E. 2012. *Machinery's Handbook 29th Edition*, New York, Industrial Press.
- RAO, S. S. 2017. *Mechanical Vibrations*, United Kingdom, Pearson Education.
- SEGEREN, M. L., LOURENS, E.-M., TSOVALAS, A. & VAN DER ZEE, T. J. 2014. Investigation of a slip joint connection between the monopile and the tower of an offshore wind turbine. *IET Renewable Power Generation*, 8, 422-432.
- SEGEREN, M. L. A. 2018. *Vibration-induced settlement of a slip-joint connection for offshore wind turbines*. PhD thesis, Delft University of Technology.
- SIF GROUP. 2018. *First offshore wind turbine using the Slip Joint connection successfully installed* [Online]. Available: <https://sif-group.com/en/news/project-updates/668-first-offshore-wind-turbine-using-the-slip-joint-connection-successfully-installed> [Accessed 20.01.20].
- SIF GROUP. n.d. *Pioneers as the basis for a green world* [Online]. Available: <https://sif-group.com/en/about-us/people-at-sif/650-pioneers-as-the-basis-for-a-green-world> [Accessed 31.01.20].
- SIMULEON. n.d. *Abaqus Standard* [Online]. Available: <https://www.simuleon.com/simulia-abagus/abagus-standard/> [Accessed 25.06.20].
- SLOCUM, R. & FAIRBAIRN, M. 2015. Slip Joints Connections—How Do These Things Work? *Electrical Transmission and Substation Structures 2015*.
- STANDARD NORGE 1992. NS-EN 40-1 Lighting columns - Part 1: Definitions and terms.
- STANDARD NORGE 2005a. Eurokode 1: Laster på konstruksjoner, Del 1-4: Almenne laster.
- STANDARD NORGE 2005b. Eurokode 3: Prosjektering av stålkonstruksjoner, Del 1-8: Knutepunkter og forbindelser
- STANDARD NORGE 2005c. Eurokode 3: Prosjektering av stålkonstruksjoner, Del 3-1: Tårn og master.
- STANDARD NORGE 2005d. NS-EN 40-2 Lighting columns - Part 2: General requirements and dimensions.
- STANDARD NORGE 2019. NS-EN 1991-1-1 Eurocode 1: Actions on structures, Part 1-1: General actions.

- STANDARDS NORWAY 2013. NORSOK N-004 Design of steel structures.
- STANDARDS NORWAY 2017. NORSOK N-003 Action and action effects.
- STORE NORSKE LEKSIKON. 2019. *Vind (English: Wind)* [Online]. Available: <https://snl.no/vind> [Accessed 18.06.20].
- TRINITY MEYER n.d. Assembly of Slipjoints.
- UNITED STATES DEPARTMENT OF AGRICULTURE 2019. Guide Specification of Standard Class Steel Transmission Poles.
- VAN DER TEMPEL, J. & LUTJE SCHIPHOLT, B. 2003. The Slip-Joint Connection, Alternative connection between pile and tower. *Dutch Offshore Wind Energy Converter project*.
- YOUNG, W. C., BUDYNAS, R. G. & SADEGH, A. M. 2011. *Roark's Formulas for Stress and Strain, Eight Edition*, United States of America, McGraw-Hill.

Appendix 1

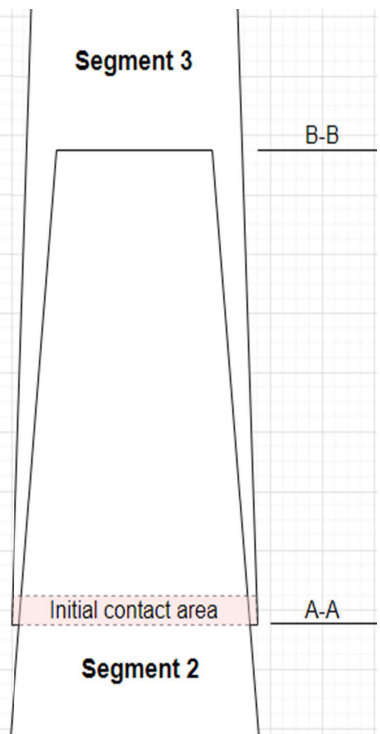
Segment	Drawing dimensions				Tapers			Pole slope angle	
	Overlap length	t	d - bottom	d - top	length	Given tap.	Calc. Tap.	from given taper	from calc. Taper
4	-	5	843	602	11700	0,02	0,02060	0,573	0,590
3	1500	6	1027	799	11100	0,02	0,02054	0,573	0,588
2	1600	8	1226	979	12000	0,02	0,02058	0,573	0,590
1	1900	10	1415	1168	12000	0,02	0,02058	0,573	0,590

Overlap of segment 2 and segment 3		
A-A	Segment 2 outer diameter	1011,9
	Segment 3 inner diameter	1015,0
	Radial gap	1,5
B-B	Segment 2 outer diameter	979,0
	Segment 3 inner diameter	982,1
	Radial gap	1,6
Axial movement for contact in A-A		149,0
Axial movement for contact in B-B		152,6

Overlap of segment 3 and segment 4		
A-A	Segment 3 outer diameter	829,8
	Segment 4 inner diameter	833,0
	Radial gap	1,6
B-B	Segment 3 outer diameter	799,0
	Segment 4 inner diameter	802,1
	Radial gap	1,6
Axial movement for contact in A-A		155,3
Axial movement for contact in B-B		150,6

Overlap of segment 1 and segment 2		
A-A	Segment 1 outer diameter	1207,1
	Segment 2 inner diameter	1210,0
	Radial gap	1,4
B-B	Segment 1 outer diameter	1168,0
	Segment 2 inner diameter	1170,9
	Radial gap	1,4
Axial movement for contact in A-A		140,5
Axial movement for contact in B-B		140,5

Unilateral convergence is given to be 10 mm/m = 0,01 for each side (written in drawings).



Appendix 2

Manual calculation of friction

1. Defining variables

Masses of the light poles are defined as stated in the technical drawings. The total mass which rests on the slip joint, stem from segment III, IV and V combined with weight of floodlights and service platforms. Mass of whole structure from 2nd splice and up:

$$m_{tot} := 4856 \text{ kg}$$

Gravitational constant:

$$g := 9.81 \frac{\text{m}}{\text{s}^2}$$

Taper:

$$taper := 20 \frac{\text{mm}}{\text{m}} = 0.02$$

Overlap length:

$$l := 1.6 \text{ m}$$

Cone angle:

$$deg := \frac{\pi}{180}$$

$$\phi := 0.59 \text{ deg}$$

$$\phi = 0.59 \text{ deg}$$

Plane inclination:

$$\theta := \frac{\pi}{2} - \phi$$

$$\theta = 89.41 \text{ deg}$$

Coefficient of friction:

$$\mu := 0.6$$

2. Calculation of friction

Gravitational force acting on splice:

$$G := m_{tot} \cdot g$$

$$G = (4.764 \cdot 10^4) \text{ N}$$

Normal force on surface:

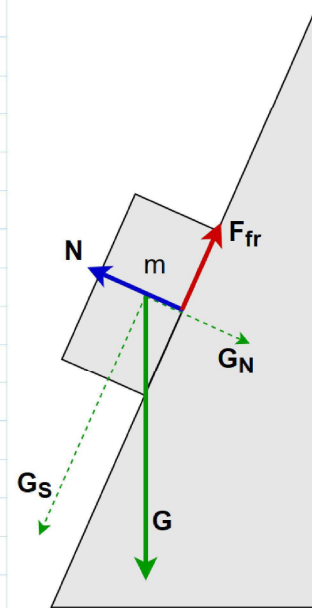
$$N := G \cdot \cos(\theta)$$

$$N = 490.534 \text{ N}$$

Friction force:

$$F_{fr} := \mu \cdot N$$

$$F_{fr} = 294.321 \text{ N}$$



The gravitational force decomposed in the direction of sliding:

$$G_s := G \cdot \sin(\theta)$$

$$G_s = (4.763 \cdot 10^4) \text{ N}$$

Checking if friction force is larger than gravitational force component in direction of sliding:

$$check := F_{fr} - G_s = -4.734 \cdot 10^4 \text{ N}$$

The gravity force component in direction of sliding is larger than the friction force, meaning that sliding will occur. The angle of repose, in this case meaning the cone angle at which sliding is just barely prevented, can be calculated from $\mu = \tan\theta$.

$$\theta_{repose} := \text{atan}(\mu)$$

$$\theta_{repose} = 30.964 \text{ deg}$$

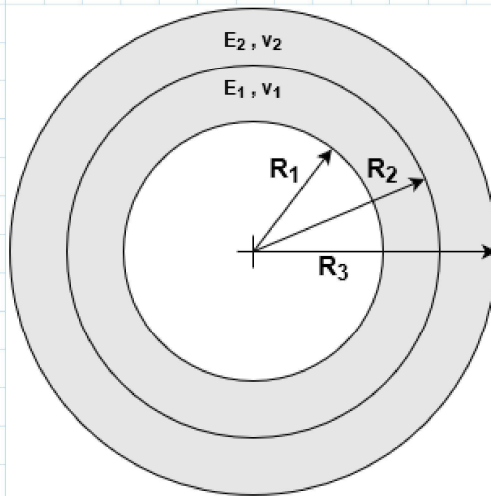
The angle required to avoid slip is not a practical solution, thus to avoid sliding an increase in normal force stemming from the interfacial pressure is needed.

Appendix 3

Manual calculation: Compound cylinder

About the calculation

The slip joint connection can be thought of as a compound cylinder. As the the slip joint segments are assembled, an interference fit is essentially formed where the inner segment of the joint is in compression and the outer segment is in tension. Following calculations are based on R.T. Fenner's *Engineering Elasticity*, p. 172-174.



$$\delta = \frac{2P(K_1^2 * K_2^2 - 1)}{E(K_1^2 - 1)(K_2^2 - 1)} * R_2$$

where:

- δ - mismatch/interference of interfacial radii before compounding
- P - interfacial pressure
- K_1 - ratio of R_2/R_1
- K_2 - ratio of R_3/R_2
- E - modulus of elasticity

Assumptions

- The pole segments are assumed to be perfectly circular, not hexadecagonal.
- Pole radii are assumed to be constant throughout the slip joint.
- The slip joint is assumed to be a thick-walled cylinder compound.
- Radii values are determined from top of segment II.
- Segment II and III are assumed to be in full contact.
- Overlap length is constant.
- Elastic properties are equal for the two components.

Defining variables

Overlap length:

$$l := 1.6 \text{ m}$$

Taper:

$$taper := 20 \frac{\text{mm}}{\text{m}} = 0.02$$

Bottom diameter of segment III:

$$d_{III_bottom} := 1027 \text{ mm}$$

Average diameter of the slip joint section is found at half the slip joint length and is here based on the outer section:

$$d_{avg} := d_{III_bottom} - taper \cdot \frac{l}{2}$$

$$d_{avg} = 1011 \text{ mm}$$

Thickness of the inner and outer cylinder:

$$t_{inner} := 8 \text{ mm}$$

$$t_{outer} := 6 \text{ mm}$$

Modulus of elasticity and Poisson's ratio for S355 J2G3 steel:

$$E := 210000 \frac{\text{N}}{\text{mm}^2}$$

$$v := 0.30$$

The coefficient of static friction for a zinc-zinc connection:

$$\mu := 0.6$$

Calculating radii of the compound cylinder:

$$R_2 := \frac{d_{avg}}{2} = 505.5 \text{ mm}$$

$$R_1 := R_2 - t_{inner} = 497.5 \text{ mm}$$

$$R_3 := R_2 + t_{outer} = 511.5 \text{ mm}$$

Calculation of ratios for adjacent radii:

$$K_1 := \frac{R_2}{R_1} = 1.016$$

$$K_2 := \frac{R_3}{R_2} = 1.012$$

Checking if nominal lap length is at least 1.5 times the average diameter of female section, length diameter ratio (LDR):

$$LDR := \frac{l}{d_{avg}} = 1.583$$

OK!

Total mass of structure above slip joint and the gravitational constant:

$$m_{tot} := 4856 \text{ kg}$$

$$g := 9.81 \frac{\text{m}}{\text{s}^2}$$

$$\theta := 89.41 \text{ deg}$$

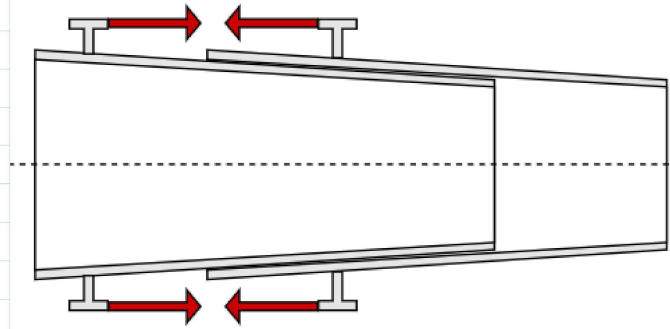
$$A := 2 \cdot \pi \cdot R_2 \cdot l = (5.082 \cdot 10^6) \text{ mm}^2$$

1. Calculation of axial movement and stresses from assembling

Axial movement during assembling

The force used to assemble the slip joint shall exceed the factored vertical compressive force that appears once the pole has been upended. From the calculation of friction the gravitational force was found to be approximately 47640 N. Therefore, a force exceeding this value multiplied by an arbitrarily selected factor of 2 is chosen:

$$F_{as} := 100000 \text{ N}$$



The assembling force component in direction of sliding:

$$F_{as_sliding} := F_{as} \cdot \sin(\theta)$$

Axial movement stops once the friction force is equal to the assembling force component in the direction of sliding:

$$F_{fr} := F_{as_sliding}$$

Interface pressure, P , is replaced by $\frac{N}{A}$ where normal force, N , is replaced by $\frac{F_{fr}}{\mu}$. The radial mismatch, δ , is then calculated by:

$$\delta := \frac{2 \cdot R_2 \cdot (K_1^2 \cdot K_2^2 - 1)}{E \cdot (K_1^2 - 1) \cdot (K_2^2 - 1)} \cdot \frac{F_{fr}}{A \cdot \mu}$$

$$\delta = 0.012 \text{ mm}$$

The calculated settlement after assembling with a force of 100000 N is found to be:

$$s_{as} := 100 \cdot \delta$$

$$s_{as} = 1.164 \text{ mm}$$

Calculation of stresses after assembling

Followingly, the stresses at radius R_2 is calculated. Variations of hoop stresses are small in the axial direction, as this compound cylinder is not thick walled per definition. ($R/t > 10$)

$$r := R_2$$

The interface pressure, P:

$$P := \frac{(E \cdot (K_1^2 - 1) (K_2^2 - 1)) \cdot \delta}{2 \cdot (K_1^2 \cdot K_2^2 - 1) \cdot R_2}$$

$$P = 0.033 \text{ MPa}$$

Cylinder 1:

$$\sigma_{rr_1} := -\frac{P}{K_1^2 - 1} \left(K_1^2 - \frac{R_2^2}{r^2} \right) = -0.033 \text{ MPa}$$

$$\sigma_{\theta\theta_1} := -\frac{P}{K_1^2 - 1} \left(K_1^2 + \frac{R_2^2}{r^2} \right) = -2.056 \text{ MPa}$$

Cylinder 2:

$$\sigma_{rr_2} := \frac{P}{K_2^2 - 1} \left(1 - \frac{R_3^2}{r^2} \right) = -0.033 \text{ MPa}$$

$$\sigma_{\theta\theta_2} := \frac{P}{K_2^2 - 1} \left(1 + \frac{R_3^2}{r^2} \right) = 2.779 \text{ MPa}$$

Ratios of hoop stress to radial stress in each cylinder:

$$r_{1s} := \left| \frac{\sigma_{\theta\theta_1}}{\sigma_{rr_1}} \right| = 62.691$$

$$r_{2s} := \left| \frac{\sigma_{\theta\theta_2}}{\sigma_{rr_2}} \right| = 84.753$$

Radial stresses are negligibly small compared to hoop stresses.

2. Calculation of interfacial pressure and stresses with axial settlement of 26 mm

Experienced settlement for one of the slip joints was found to be 26 mm:

$$s_{26} := 26 \text{ mm}$$

Mismatch increase at distance s further down the conical pole:

$$\Delta\delta := s_{26} \cdot \frac{\text{taper}}{2} = 0.26 \text{ mm}$$

Mismatch as result of settlement after assembling:

$$\delta_{s26} := \delta + \Delta\delta = 0.272 \text{ mm}$$

The increased mismatch produces an increased interface pressure:

$$P_{s26} := \frac{(E \cdot (K_1^2 - 1) (K_2^2 - 1)) \cdot \delta_{s26}}{2 \cdot (K_1^2 \cdot K_2^2 - 1) \cdot R_2} = 0.765 \text{ MPa}$$

New hoop stresses at R_2 due to increased mismatch:

$$\sigma_{\theta\theta_1} := -\frac{P_{s26}}{K_1^2 - 1} \left(K_1^2 + \frac{R_2^2}{r^2} \right) = -47.981 \text{ MPa}$$
$$\sigma_{\theta\theta_2} := \frac{P_{s26}}{K_2^2 - 1} \left(1 + \frac{R_3^2}{r^2} \right) = 64.866 \text{ MPa}$$

Expectedly, the hoop stresses in the inner segment of the slip joint, $\sigma_{\theta\theta_1}$, is negative as it is in compression. $\sigma_{\theta\theta_2}$ is positive as the pole is in tension. Their absolute values are increasing in magnitude with increasing settlement. Similarly, the surface pressure increases between the two components, which results in larger normal force.

$$N := P_{s26} \cdot A$$

$$N = (3.889 \cdot 10^6) \text{ N}$$

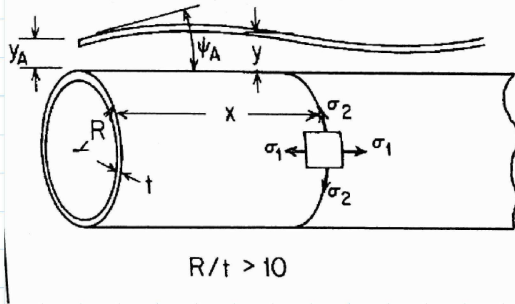
$$F_{fr} := \mu \cdot N = (2.334 \cdot 10^6) \text{ N}$$

This friction force is well beyond Gs, meaning that other effects than just gravitational forces has caused the axial settlement.

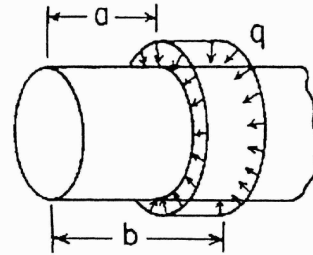
Appendix 4

Roark's formulas for stress and strain, thin-walled cylindrical shells under axisymmetric loading

Long shells with the left end free (right end more than $6/\lambda$ unit of length from the closest load)



12. Uniform radial pressure from a to b



$$\text{Radial deflection} = y = y_A F_1 + \frac{\Psi_A}{2\lambda} F_2 + L T_y$$

$$R := 0.5135 \text{ m}$$

$$t := 6 \text{ mm} = 0.006 \text{ m}$$

$$\nu := 0.3$$

$$E := 210000 \frac{\text{N}}{\text{mm}^2} = (2.1 \cdot 10^{11}) \frac{\text{N}}{\text{m}^2}$$

$$c := 0 \text{ mm}$$

$$l := 11100 \text{ mm} = 11.1 \text{ m}$$

$$a := 9500 \text{ mm} - c = 9.5 \text{ m}$$

$$b := 11100 \text{ mm} - c = 11.1 \text{ m}$$

right end more than $6/\lambda$ from the closest load.

$$\lambda := \left(\frac{3 \cdot (1 - \nu^2)}{R^2 \cdot t^2} \right)^{\frac{1}{4}}$$

$$\lambda = 23.158 \frac{1}{\text{m}}$$

$$D := \frac{E \cdot t^3}{12 \cdot (1 - \nu^2)}$$

$$D = (4.154 \cdot 10^3) \text{ J}$$

If $x < a$, $\langle x-a \rangle^0 = 0$; if $x > a$, $\langle x-a \rangle^0 = 1$; (Unit Step Function)

Any pressure can be selected, therefore the surface pressure from Manual calculation 2 is used, i.e. at 26 mm settlement

$$q := -0.77 \frac{N}{mm^2}$$

$$x := 9 \text{ m}, 9.01 \text{ m} \dots 10.9 \text{ m}$$

$$x := x = \begin{bmatrix} 9 \\ 9.01 \\ 9.02 \\ 9.03 \\ 9.04 \\ 9.05 \\ 9.06 \\ 9.07 \\ 9.08 \\ 9.09 \\ 9.1 \\ 9.11 \\ \vdots \end{bmatrix} \text{ m}$$

$$f_{step}(x, a) := \begin{cases} 0 & x < a \\ 1 & x > a \end{cases}$$

$$F_1 := \overline{\cosh(\lambda \cdot x) \cdot \cos(\lambda \cdot x)}$$

$$F_2 := \overline{\cosh(\lambda \cdot x) \cdot \sin(\lambda \cdot x)} + \overline{\sinh(\lambda \cdot x) \cdot \cos(\lambda \cdot x)}$$

$$F_{a1} := \overline{f_{step}(x, a) \cdot \cosh(\lambda \cdot (x - a)) \cdot \cos(\lambda \cdot (x - a))}$$

$$F_{a5} := f_{step}(x, a) - F_{a1}$$

$$F_{b1} := \overline{f_{step}(x, b) \cdot \cosh(\lambda \cdot (x - b)) \cdot \cos(\lambda \cdot (x - b))}$$

$$F_{b5} := f_{step}(x, b) - F_{b1}$$

$$A_2 := \frac{1}{2} \cdot e^{(-\lambda \cdot a)} \cdot (\sin(\lambda \cdot a) - \cos(\lambda \cdot a))$$

$$B_2 := \frac{1}{2} \cdot e^{(-\lambda \cdot b)} \cdot (\sin(\lambda \cdot b) - \cos(\lambda \cdot b))$$

$$LT_y := \frac{-q}{4 \cdot D \cdot \lambda^4} (F_{a5} - F_{b5})$$

$$A_3 := -\frac{1}{2} \cdot e^{-\lambda \cdot a} \cdot \sin(\lambda \cdot a)$$

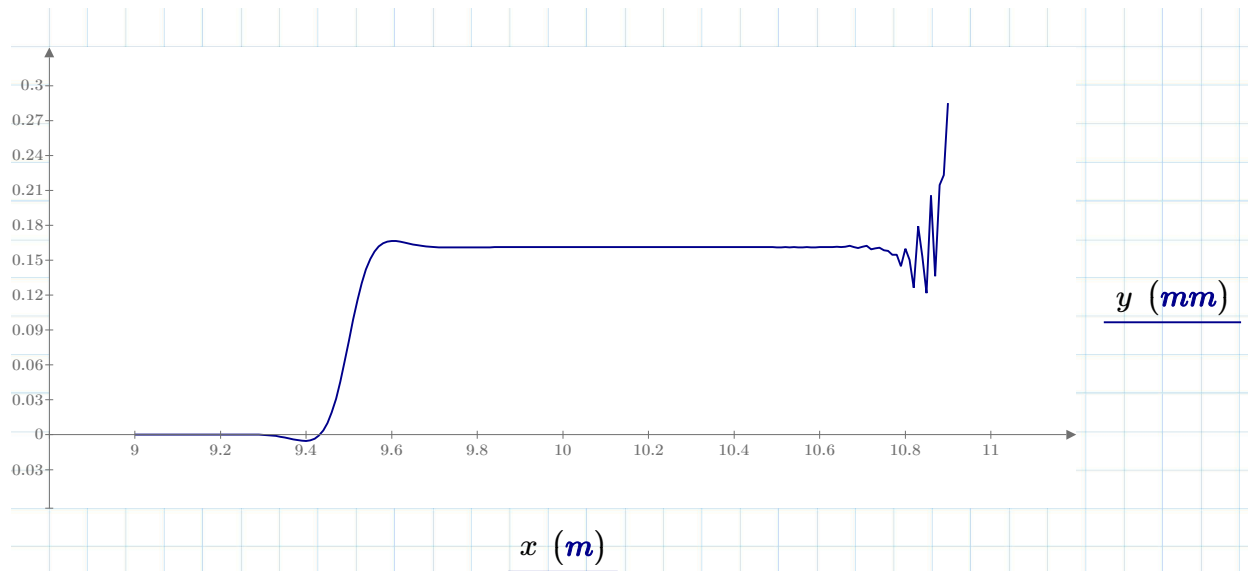
$$B_3 := -\frac{1}{2} e^{-\lambda \cdot b} \cdot \sin(\lambda \cdot b)$$

$$y_A := \frac{-q}{2 \cdot D \cdot \lambda^4} (B_2 - A_2) = (4.192 \cdot 10^{-100}) \text{ m}$$

$$\Psi_A := \frac{-q}{D \cdot \lambda^3} \cdot (B_3 - A_3) = 1.84 \cdot 10^{-99}$$

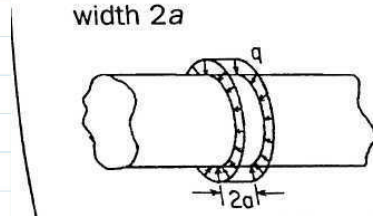
$$y := y_A \cdot F_1 + \frac{\Psi_A}{2 \cdot \lambda} \cdot F_2 + LT_y$$

$$y = \begin{bmatrix} 4.154 \cdot 10^{-7} \\ 3.276 \cdot 10^{-7} \\ 1.436 \cdot 10^{-7} \\ -1.681 \cdot 10^{-7} \\ -6.407 \cdot 10^{-7} \\ -1.305 \cdot 10^{-6} \\ -2.184 \cdot 10^{-6} \\ -3.286 \cdot 10^{-6} \\ -4.593 \cdot 10^{-6} \\ -6.048 \cdot 10^{-6} \\ -7.543 \cdot 10^{-6} \\ -8.899 \cdot 10^{-6} \\ \vdots \end{bmatrix} \text{ mm}$$



Using formulas for "very long shells" where both ends are more than $6/\lambda$ units of length from the nearest loading:

17. Uniform pressure over a band of width $2a$



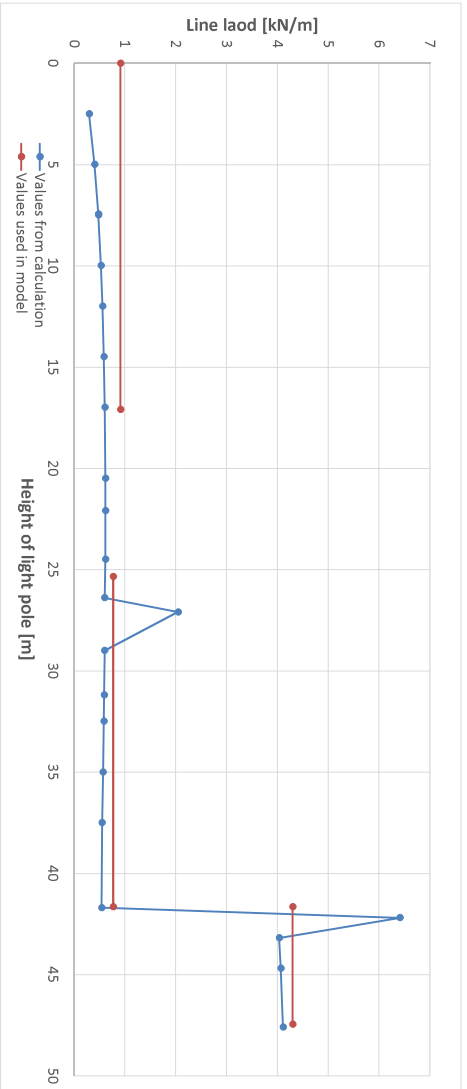
$$y_{max} := \frac{-q}{4 \cdot D \cdot \lambda^4} (1 - e^{-\lambda \cdot a} \cdot \cos(\lambda \cdot a)) = 0.161 \text{ mm}$$

"The original differential equations used to develop the formulas presented in Table 3.2 were based on the assumption that radial deformations were small. If the magnitude of the radial deflection approaches the wall thickness, the accuracy of the equations declines." (Roarks, p.579)

Appendix 5

Calculation of wind loads

#	Velocity $V_{0,0}$ m/s	Reference velocity $V_{0,r}$ m/s	Altitude factor C_{alt}	Directional factor C_{dir}	Seasonal factor C_{season}	Velocity $V_{0,r}$ m/s	K	terrain factor	Roughness length z_0 m	Minimum height z_{min} m	Height z m	Mean speed, 10 min V_m	Wind turbulence I_z	Basic velocity $q_{b,r}$ N/m ²	Peak velocity pressure $q_{p,r}$ N/m ²	CSCD	D, m	Damping	Wind force factor F_{w1}	Wind force factor F_{w2}	Shear force factor F_{s1}	Total wind force moment for F_{w1}	Total wind force moment for F_{w2}
1	26	30	1,08	1	1	28,08	0,19	0,05	0,05	4	47,6	36,59	0,146	866,64	1749,13	0,76	0,479	71,1	5,43	4,11	11,92	749,6	567,4
2	26	30	1,08	1	1	28,08	0,19	0,05	0,05	4	44,7	36,26	0,147	849,84	1725,24	0,75	0,545	70,5	5,43	4,07	11,92	749,6	567,4
3	26	30	1,08	1	1	28,08	0,19	0,05	0,05	4	43,2	36,07	0,148	841,33	1712,32	0,75	0,572	70,1	5,42	4,04	11,92	749,6	567,4
4	26	30	1,08	1	1	28,08	0,19	0,05	0,05	4	42,2	35,95	0,148	835,51	1703,49	0,74	0,591	69,9	8,64	6,41	3,21	182,3	135,3
5	26	30	1,08	1	1	28,08	0,19	0,05	0,05	4	41,7	35,92	0,151	806,48	1659,25	0,73	0,721	68,6	0,74	0,54	2,27	129,6	94,6
6	26	30	1,08	1	1	28,08	0,19	0,05	0,05	4	37,5	35,32	0,151	789,76	1633,64	0,72	0,767	67,9	0,75	0,57	1,37	70,7	54,4
7	26	30	1,08	1	1	28,08	0,19	0,05	0,05	4	35	34,95	0,153	771,99	1606,33	0,71	0,814	67,2	0,79	0,57	1,42	69,1	49,7
8	26	30	1,08	1	1	28,08	0,19	0,05	0,05	4	32,5	34,56	0,154	771,99	1606,33	0,71	0,814	67,2	0,82	0,58	0,76	34,8	24,7
9	26	30	1,08	1	1	28,08	0,19	0,05	0,05	4	31,2	34,34	0,155	762,29	1591,37	0,70	0,838	66,7	0,84	0,59	1,30	57,7	40,6
10	26	30	1,08	1	1	28,08	0,19	0,05	0,05	4	29	33,99	0,159	729,29	1540,21	0,69	0,914	65,3	0,86	0,60	1,14	47,4	33,1
11	26	30	1,08	1	1	28,08	0,19	0,05	0,05	4	27,1	33,59	0,159	729,29	1540,21	0,69	0,914	65,3	0,90	0,60	1,43	56,5	38,8
12	26	30	1,08	1	1	28,08	0,19	0,05	0,05	4	26,4	33,50	0,161	706,10	1504,04	0,67	0,962	64,2	0,90	0,61	1,14	45,1	30,1
13	26	30	1,08	1	1	28,08	0,19	0,05	0,05	4	24,5	33,05	0,161	682,80	1467,45	0,66	1,006	63,2	0,91	0,61	1,47	53,6	36,1
14	26	30	1,08	1	1	28,08	0,19	0,05	0,05	4	22,1	32,50	0,164	666,05	1441,03	0,65	1,036	62,4	0,93	0,62	0,99	42,9	21,8
15	26	30	1,08	1	1	28,08	0,19	0,05	0,05	4	20,5	32,10	0,166	666,05	1441,03	0,65	1,036	62,4	0,94	0,61	2,15	67,5	44,0
16	26	30	1,08	1	1	28,08	0,19	0,05	0,05	4	17	31,10	0,172	625,24	1376,10	0,63	1,100	60,4	0,95	0,60	1,50	40,5	25,5
17	26	30	1,08	1	1	28,08	0,19	0,05	0,05	4	14,5	30,25	0,176	591,59	1321,95	0,61	1,147	58,8	0,96	0,58	1,46	34,6	21,1
18	26	30	1,08	1	1	28,08	0,19	0,05	0,05	4	12	29,24	0,182	552,75	1258,75	0,59	1,193	56,8	0,95	0,56	1,11	22,7	13,4
19	26	30	1,08	1	1	28,08	0,19	0,05	0,05	4	10	28,27	0,189	516,59	1199,10	0,57	1,230	54,9	0,93	0,53	1,32	23,2	13,2
20	26	30	1,08	1	1	28,08	0,19	0,05	0,05	4	7,5	26,73	0,200	462,01	1107,46	0,53	1,276	52,0	0,89	0,48	1,02	0,3	0,2
21	26	30	1,08	1	1	28,08	0,19	0,05	0,05	4	7,45	26,70	0,200	460,78	1105,37	0,53	1,277	51,9	0,89	0,47	1,16	16,2	8,7
22	26	30	1,08	1	1	28,08	0,19	0,05	0,05	4	5	24,57	0,217	390,27	983,48	0,49	1,322	47,8	0,82	0,40	1,01	10,2	5,0
23	26	30	1,08	1	1	28,08	0,19	0,05	0,05	4	2,5	20,87	0,228	281,63	731,51	0,47	1,369	40,6	0,63	0,30	0,74	3,9	1,8



Segment	Moment KNm	Shear force KN	Line load applied to KN/m
5	1149.7	25.80	4.30
Top beam	420.79	12.56	0.77
Bottom beam	132.96	15.55	0.91